Estimation and mapping of forest biomass and carbon using point-clouds derived from airborne LiDAR and from 3D photogrammetric matching of aerial images

Aruna Thapa Magar
June, 2014

Course Title:	Geo-Information Science and Earth Observation for Environmental Modelling and Management
Level:	Master of Science (MSc)
Course of Duration:	August 2012 – June 2014

Consortium Partners:

Lund University, (Sweden)
University of Twente,
Faculty of ITC (The Netherlands)
University of Southampton, (UK)
University of Iceland, (Iceland)
University of Sydney,
(Australia, Associate partner)

Estimation and Mapping of forest biomass and carbon using point-clouds derived from airborne LiDAR and from 3D photogrammetric matching of aerial images

by

Aruna Thapa Magar

Thesis submitted to the faculty of Geo-Information Science and Earth Observation (University of Twente) in partial fulfilment of the requirements for the degree of Master of Science in Geo-information Science and Earth Observation, Specialisation: Environmental Modelling and management.

Thesis Assessment Board

Prof. Dr. A. K. Skidmore (Chair)
Dr. M. Gerke (External examiner, Department of Earth Observation Science, ITC)

Dr. M. J.C. Weir (First Supervisor)
Dr. Y. A. Hussin (Second Supervisor)

ITC UNIVERSITY OF TWENTE.
FACULTY OF GEO-INFORMATION SCIENCE AND EARTH OBSERVATION

Disclaimer

This document describes work undertaken as part of a programme of study at the Faculty of Geo-Information Science and Earth Observation (University of Twente). All views and opinions expressed therein remain the sole responsibility of the author, and do not necessarily represent those of the institute.

Abstract

Accurate assessment and monitoring of forest biomass is important for sustainable forest management. In particular, biomass assessment is required to estimate the global carbon budget, which is affected by recent increases in atmospheric CO_2 concentrations. Various remote sensing (RS) techniques can be applied to estimate forest biomass. Airborne LiDAR data, in this respect, has proved to be a valuable tool, able to provide accurate estimates of above-ground biomass (AGB). Similarly, three-dimensional (3D) matching of digital aerial photographs provides a new prospective for AGB estimation which is low cost compared to LiDAR. This study aims to compare the photogrammetric 3D aerial point cloud and LiDAR to extract tree height and Crown Projection Area (CPA) and develop species-specific regression models for accurate estimation and mapping of carbon stock in Bois noir forest of Barcelonnette, France. LiDAR data was processed to obtain the canopy height model (CHM) by subtracting the digital terrain model (DTM) from digital surface model (DSM). 3D aerial point clouds were processed to generate CHM using subtraction of LiDAR DTM from aerial DSM since the terrain does not change abruptly but gradually. Tree crown delineation was done using a region growing approach in object based image analysis (OBIA). The carbon stock was calculated from field measured DBH and height using species-specific allometric equations and a standard conversion factor. For carbon stock estimation and mapping of the study area, species-wise multiple regression models were developed using segmented CPA and derived CHM from LiDAR and aerial point clouds and field measurements. The LiDAR derived tree height and the CHM derived from aerial point clouds were able to explain 81% and 66% of the field measured height variability respectively. Overall segmentation accuracy was 77% and 80% based on 1:1 correspondence for LiDAR and aerial image respectively. Species wise multiple regressions were able to explain 57%, 74%, 84% & 88% of variation in carbon estimation for *Pinus uncinata, Pinus sylvestris, Fagus sylvatica* and *Larix decidua* in the case of the aerial image and 54%, 57%, 71% & 72% of variation in the case of the LiDAR. A total of 54.18 tonne C ha^{-1} and 47.37 tonne C ha^{-1} AGB carbon stock was estimated using aerial images and LiDAR respectively. This study concludes that photogrammetric matching of digital aerial images is as promising a technique as LiDAR for estimating above ground carbon stock and the cost of forest sampling can be reduced with its application.

Acknowledgements

I am very grateful to all those who contributed to the successful completion of this research work. I would like to express my sincere gratitude to my first supervisor Dr. Michael Weir, for his continuous encouragement, invaluable suggestions, constructive feedback and comments from the very beginning till the completion of this research. It was a real opportunity and pleasure to work under his supervision. I also like to extend my deepest gratitude to my second supervisor Dr. Yousif Hussin who introduced this wonderful research topic to me and providing valuable advice and guidance during field work conduction as well as feedback during my study. Without my supervisors' guidance, this research would hardly have come to fruition.

It is my immense pleasure to extend my profound appreciation to Dr. Markus Gerke for his valuable support and assistance in generating photogrammetric point cloud using Pix4D. My sincere thanks go to Prof. Andrew Skidmore, for his critical comments and suggestions during the proposal writing.

I am deeply honoured and would like to acknowledge the European Union Erasmus Mundus GEM scholarship program for providing me an opportunity to pursue my MSc Degree at Lund University, Sweden and the ITC, University of Twente, Netherlands. I had an amazing multicultural experience.

Special acknowledgement goes to Mercy Ndalila who accompanied me to the field and support in many ways sharing together both tough and cheerful moments. I would also like to express my great appreciation to my GEM friends Fatimeh, Nina, Phibion, Milena, Dariya and Karolina for their moral support and quality time spent while in Lund. My sincere thanks also go to my fellow NRM friends for their valuable advices and encouragements during the research.

I sincerely owe gratitude to Ms. Anahita Khosravipour who provided technical guidance and knowledge on operating LAStools© for processing LiDAR data. My sincere appreciation also goes to my friends Apri Dwi Sumarah and Jarot Pandu Panji Asmoro for their support during the research.

I am very much thankful to Rehana, Sweta and Shrota and to all the Nepalese friends (NEPALI SAMAJ), who really kept a homely environment and shared joyful moments during my stay at Europe.

Finally, deepest appreciation goes to my parents, my brother and sisters and the rest of my family members who always encourage me and wish for my success.

Aruna Thapa Magar
Enschede, Netherlands
June 2014

Table of Contents

List of figures

List of tables

Chapter 1

1.1 INTRODUCTION

1.1.1 Background

Forest ecosystems play a very important role in the global carbon cycle, contributing 80% of all above-ground and 40% of all below ground terrestrial organic carbon (Kirschbaum, 1996). Forest biomass which is defined as "the dry mass of the above-ground portion of live trees per unit area" (Bonnor, 1985) is linked to many forest ecosystem processes. The growth in forest biomass results in net atmospheric carbon sequestration in the terrestrial biosphere whereas the cutting or burning of forest causes emissions to the atmosphere. Forests, therefore, act as either a carbon sink or source. The increasing concentration of atmospheric carbon dioxide (CO_2), the major constituent of Green House Gases (GHG) is one of the main causes of climate change (IPCC, 2007). With the growing awareness about rising CO_2 concentrations, the role of forests in the assimilation of atmospheric CO_2 is being increasingly realized. The preservation of forest areas can contribute strongly to the mitigation of global climate change. Therefore, for understanding the global carbon cycle, the assessment of carbon stock is crucial and are highly practiced (Sierra et al., 2007).

Quantifying biomass is a matter of significant concern within the United Nations Framework Convention on Climate Change (UNFCC) and the Kyoto Protocol, both of which require signatory countries to regularly assess and address the issue of reducing GHG emissions in the atmosphere. All the contracting parties to the UNFCC convention commit themselves to update, publish and report their national inventories to emissions by sources and removals of sinks of all GHGs (Houghton, 1997). The Bali Action Plan of UNFCC in 2007 opened opportunities for developing countries to participate in forest carbon financing through the mechanism of "Reducing Emission from Deforestation and forest Degradation" (REDD). This aims to reduce emissions from forested lands by minimizing carbon emissions and investing in low-carbon paths of sustainable development (MOFSC, 2009). Thus. REDD is an international effort to create a financial value for the carbon stored in forests.

Forest management relies on accurate and up-to-date spatial information for the assessment of forest resources and for planning forest management activities (Weir, 2000). It is widely recognized that obtaining different forest parameters through ground measurements is time consuming and costly. Aerial photography, spaceborne optical sensors, Radar and LiDAR are used in collecting spatial data (Suárez, 2002). These remote sensing techniques are used as indirect methods that are capable of obtaining information efficiently over wide areas.

1.1.2 Overview of techniques for biomass estimation

There are different techniques to measure biomass of forest. The main three techniques can be categorized as i) field measurement based (Brown et al., 1989), ii) GIS based (Brown & Gaston, 1996) and iii) Remote Sensing based (Lu, 2006) approaches. The traditional approaches based on field measurements are accurate, but their application is limited due to their laborious and destructive nature. GIS based methods, in the absence of good quality ancillary data such as land cover type, site quality and forest age, etc. are difficult because of an indirect relationship between these ancillary data and biomass in an area and the comprehensive impacts of environmental conditions on biomass accumulation. RS based method do not measure biomass directly, but rather use the statistical relationship between tree parameters extracted from satellite or aerial images and ground based measurements. This makes RS based approaches a faster method than the other approaches for the estimation of biomass (Gibbs et al., 2007).

The majority of biomass assessments are done for above-ground biomass (AGB) of trees. The AGB accounts the greatest fraction of total living biomass in a forest which can be measured directly in the field or indirectly through emote sensing technique. The determination of biomass typically involves measurements of tree size parameters, in particular trunk diameter at breast height (DBH) and tree height. DBH is the stem diameter of a tree at 1.3 m above the ground level. DBH and height are the important tree parameters for biomass estimation (Jenkins et al., 2003). These parameters are used to develop allometric equations to estimate biomass. Since, DBH can be more easily measured in the field than height, most of the allometric equations are developed based on DBH (Jenkins et al., 2003). Allometric equations are the most used tool to assess the volume or biomass from forest inventory data. The quality of these equations is crucial for ensuring the accuracy of forest carbon estimates. However, the propagation of errors all along the process of building these equations should be considered, from the field work to the modelling and the prediction (Nguyet, 2012; Picard et al., 2012). Wood density is also an important variable in order to assess the biomass, which is defined as "the ratio of dry biomass with the fresh volume without bark" (IPCC, 2006).

Aerial photography and its applications for forest characteristics estimation

Aerial photography is the economical method of RS for taking pictures of earth surface from an airborne platform such as aircraft, helicopter, kite and unmanned aerial vehicle (UAV). 2D or 3D models are created from aerial photographs of the ground from an elevated position and the technique is termed as aerial photogrammetry. Photogrammetric techniques are used to accurately determine the relationships of features on aerial photographs, such as ground distances and angles, the heights of objects and terrain elevations (Natural Resources Canada, 2007).

Aerial photographs are classified into vertical and oblique photos, and they can be captured depending on the application intended. In vertical photos, the optical axis of the camera is perpendicular to the ground while, in oblique photos, the axis of the photograph is purposely tilted from the vertical. Most photographs are acquired vertically down from the aircraft so that measurements of objects and areas on Earth's surface can be made with a minimum of calculation and correction for distortion due to the tilt of the camera. The photos are taken with overlap within flight-lines (forward overlap) and between flight-lines (sidelap). Forward overlap within a flight-line typically is from 60 to 70% while sidelap between flight-lines typically is from 25 to 40% (Wolf & Dewitt, 2000) (Figure 1). Aerial photography is acquired with significant (more than 50%) overlap between images to obtain a complete 3D view of the covered territory (stereoscopic overlap), which can be viewed using a stereoscope. Through the use of photogrammetry, highly detailed 3D data can be derived from 2D photographs of a stereo pair. The 3D view is made possible by the effect of parallax, which refers to the apparent change in relative positions of stationery objects caused by a change in viewing position (Murtha & Sharma, 2005). Measurements of this parallax are used to deduce the height of the objects.

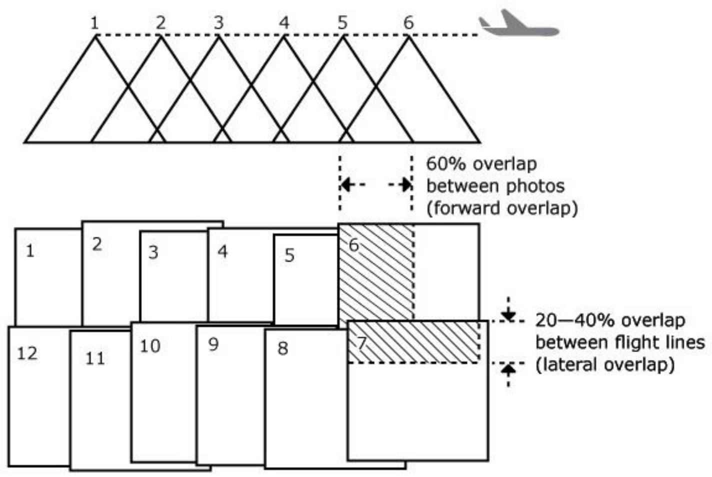

Figure 1: Illustration of flight line and image overlapping
Source: Natural Resources Canada (www.nrcan.gc.ca)

The paradigm shift in aerial photogrammetry from analogue to digital photogrammetry has made aerial photography a rapidly evolving tool for environmental and ecological management. Digital photogrammetry is a computerized application and can be used with digital images and scanned analogue photographs (Madani, 2001). Digital aerial cameras have much higher radiometric resolution than analogue aerial cameras. The digital aerial photographs can be interpreted as 2D and 3D image. 3D based interpretation develops with digital photogrammetry can produce many forest parameters such as tree height, canopy density, crown radius and crown surface curvature (Gong et al., 2002). The recent advancement in algorithms to generate 3D data from automatic matching of aerial imagery has created a revolution in the estimation of forest parameters (Bohlin et al., 2012).

Although aerial photography was used for forest mapping in Myanmar in the 1920s, its widespread use as a major tool in forestry and related fields came about in the United States in the 1940s (Avery, 1969; Morgan et al., 2010). Aerial photography has been the most used RS data for decades in assessment, inventory and monitoring of natural resources (Packalen, 2009). Korpela (2004) lists the applications of photogrammetry in forestry such as forest mapping, stand attribute estimation, forest damage evaluation, interpretation of individual tree characteristics and tree composition estimation. Digital aerial photographs having multispectral information at the red, green, blue and near-infrared levels and high spatial resolution can be useful for acquiring tree species composition at individual tree or stand level (Kim et al., 2010). Similarly, many researchers have used analogue and digital aerial photographs to estimate different forest parameters such as volume measurement (Aldred, 1978), canopy structure (Nakashizuka et al., 1995), cover and distribution (Hudak & Wessman, 2001), stand biomass in tropical forest (Okuda et al., 2004), AGB in temperate forest (Tiwari & Singh, 1984). Nowadays, Unmanned Aerial Vehicles (UAVs) are rapidly gaining popularity for resource management due to the flexibility and relatively low cost for image acquisition. Thus, researchers are testing UAV in many forestry applications such as forest resources assessment (Herwitz et al., 2004), forest fire monitoring (Merino et al., 2012) and forest characterization (Tao et al., 2011).

Satellite Imagery and its application

Many studies have been carried out to estimate forest AGB using various types of RS satellite imagery at various scales and environments. The coarse spatial resolution optical sensors such as NOAA AVHRR (Dong et al., 2003) and MODIS (Baccini et al., 2004) have been used for estimating biomass for the global, continental and national scales. On the other hand, because of the mixed pixels and a huge difference between the support of ground reference data and pixel size of the satellite data, the application of coarse resolution NOAA AVHRR have been limited (Lu et al., 2003). For regional and local scale, medium resolution satellite imagery, such as Landsat TM, is routinely used to estimate AGB (Steininger, 2000). However, these optical remote sensing technologies face the problem of cloud cover, which limits the acquisition of high quality RS data (Karna, 2012). Very high resolution (VHR) satellite images have been used to develop carbon for carbon estimation of the forest (Shrestha, 2011). However, the effect of shadow, sun elevation angle and off-nadir viewing angle cannot be tackled by the high resolution satellite images.

LiDAR and its applications in forestry

Light Detection and Ranging (LiDAR) is a relatively recent active RS technology for high precision three dimensional (3D) topographic data acquisition (Lefsky et al., 2002). Airplanes and helicopters are the most commonly used platforms for acquiring LiDAR data over broad areas (Figure 2). The LiDAR device directly measures the distance between the sensor and the target surface. It determines the elapsed time between the emission of laser pulse and the detection of the reflected signal (the return signal) at the sensor's receiver (Jensen, 1996). The laser pulse is emitted from the device and travels through the atmosphere into a forested area and is then reflected from several surfaces such as a canopy, branches, leaves and often the ground (Evans et al., 2009). A laser pulse is in the near infrared or visible part of the electromagnetic spectrum (900 – 1064 nm). For canopy mapping or studying forest parameters, LiDAR data often are acquired in leaf-off conditions to maximize the laser returns from tree crowns and forest structures (McGaughey & Carson, 2003).

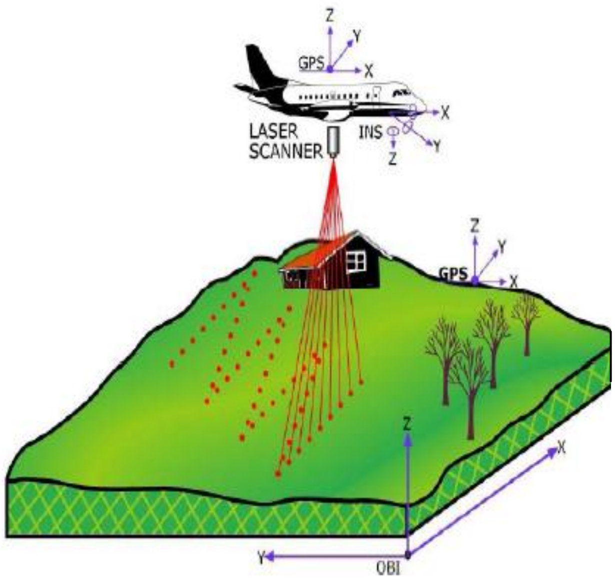

Figure 2: Airborne LiDAR data acquisition (USDA, 2006)

LiDAR system consists of four precision instruments: (1) a global positioning system (GPS), (2) an inertial navigation system (INS), and (3) an angle encoder and (4) a clock

The absolute position of reflective surfaces such as the tree canopy, understory vegetation and the ground surface are recorded by LiDAR through the combination of these four elements. The GPS provides the coordinates of the laser source and the INS measures the attitude (roll, pitch and yaw) of the sensor. The angle encoder helps in measuring the orientation of the scanning mirror while the clock measures the time between when a pulse is emitted and received (Lefsky et al., 2002). A detailed group of elevation points, called a "point cloud" are generated when laser ranges are combined with position and orientation data that are obtained from the abovementioned integrated elements. Each point in the point cloud has 3D spatial coordinates that correspond to a particular point on the Earth's surface from which a laser pulse was reflected. The point cloud conveys information on elevation, structural geometry and intensity.

LiDAR sensor can be categorized into two forms i.e. Discrete-return devices and Waveform recording device for receiving laser pulse returns. Discrete-return systems have a high spatial resolution which detects fine-scale or 'small-footprint' variation (typically 20 – 80 cm in diameter). These are able to record one to several returns through the forest canopy depending on returned laser intensity to a sensor. In contrast, waveform systems lack the spatial resolution resulting in a 'large-footprint' variation (10 – 100 m). This records the amount of energy returned to the sensor for a series of equal time intervals (Evans et al., 2009). The distinction between discrete-return and waveform LiDAR is illustrated in Figure 3.

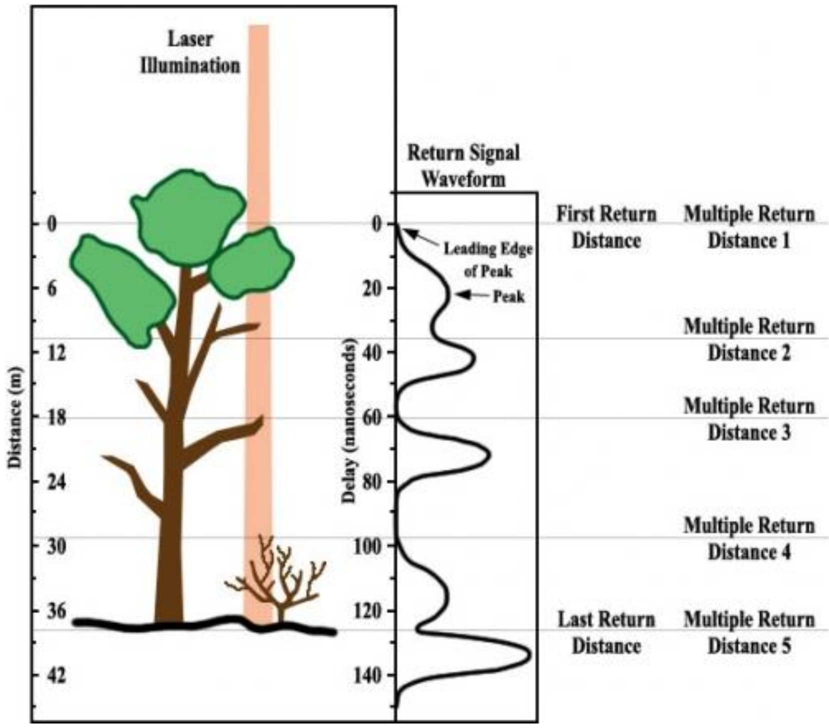

Figure 3: Illustration of the conceptual differences between waveform and discrete-return LiDAR devices (Lefsky et al., 2002)

LiDAR is considered to be a promising technique for forest monitoring because of its ability to assess the 3D forest structure (Patenaude et al., 2005) and to provide a reliable data on vertical profiles of vegetation canopies (Balzter et al., 2007). With this capability, various methods have been developed for biomass estimation using both discrete-return and full waveform LiDAR systems. Lim and Treitz (2004) reviewed and found the potential of LiDAR for retrieving forest parameters. LiDAR data have been used to study several biophysical forest metrics such as Douglas fir western hemlock biomass (Means et al., 1999), tropical forest biomass (Drake et al., 2002), tree height and stand volume (Nilsson, 1996), tree crown diameter (Popescu et al., 2003), and canopy structure (Lovell et al., 2003). Lefsky et al. (2001) explained 84% of the AGB variance by regression from the LiDAR measured canopy structure. Popescu (2007) developed a method for biomass extraction from LiDAR-derived tree height and crown diameter in combination with regression models at individual tree level where she found the good model performance with R^2 of 0.93. Ke et al. (2010) performed forest classification with an accuracy of 87% using LiDAR based segmentation. LiDAR complements traditional field methods through data analysis, which is an advantage over high resolution satellite imagery for the extraction of vegetation parameters in detail (Song et al., 2010). These systems have been used either alone or in combination with passive optical or RaDAR data (Hyde et al., 2007). Fusion of LiDAR and very high resolution optical images show promise and can offer substantial improvements to biomass estimates (Chen et al., 2012; Erdody & Moskal, 2010).

1.1.3 Point cloud based on aerial image and LiDAR

A point cloud is "a set of geometrically unstructured observations consisting of a large number of individual measurements in a three-dimensional coordinate system" (Heritage & Large, 2009). Both LiDAR and aerial imagery have been employed in many application fields because they generate reliable and dense 3D point clouds over subjects or surfaces under consideration. Photogrammetry has a long history for the automation of information extraction from digital images while LiDAR is a more recent technology (Baltsavias, 1999). Despite the fact that tools for automatic stereo image matching have been available for more than decades, the collection of high resolution, high accuracy elevation data has been mainly dominated by the application of airborne LiDAR systems (Haala, 2009). However, automatic generation of high quality, dense point clouds from digital images by matching is a recent technology in digital photogrammetric technology (Haala, 2009). Lemaire (2008) reports that a DSM can be generated from image matching having similar accuracy to that of high resolution LiDAR data.

DSM and DTM generated from aerial images provide sufficient accuracy to manage forest resources. Waser et al. (2008) used a photogrammetric DSM to detect the tree/shrub on a mire environment. St-Onge (2008) combined LiDAR and digital photogrammetry to create hybrid photo LiDAR CHMs where LiDAR was used to produce a DTM and a DSM was obtained using automatic stereo matching of aerial photographs. This kind of study opens up the possibility of using historical photography to retrospectively assess biomass (Morgan et al., 2010). A number of studies have shown the successful use of LiDAR combined with other sensor data to estimate tree height, crown diameter, basal area, stem volume and mapping the 3D canopy structure as canopy height models (Næsset & Gobakken, 2005). Some of the studies using LiDAR and aerial imagery either alone or in combination were shown in Table 1 to produce timely and accurate forest parameters.

The high point density of LiDAR data makes it more possible to detect accurate height and crown dimensions of individual trees. Persson et al. (2002) detected height and crown diameter with RMSE of 0.63 m and 0.61 m respectively with high density of points. Kwak et al. (2010) estimated the stem volume and biomass of individual *Pinus koraiensis* using LiDAR with density of 5-7 point/m^{-2}. An individual tree crown and height of deciduous forest was analysed by (Brandtberg et al., 2003) using point density of 12 point/m^{-2}. In their study, (Thomas et al., 2006) found that the high density models are well correlated with mean dominant tree height (0.90), basal area (0.91) and crown closure (0.92) while crown closure could not be predicted accurately with low density models. In many research studies, LiDAR data fusion, especially low point density with high resolution aerial imagery or passive optical sensors, is considered to be effective. For example, improving measurement of forest structural parameters by co-registering aerial imagery and LiDAR data (Huang et al., 2009). The integration of digital aerial photography and LiDAR data can be more useful for assessing biomass and carbon storage than using either aerial photographs or LiDAR data alone (Popescu, 2007).

Table 1: Application of LiDAR and aerial photos

Author	**Aerial image**	**LiDAR**	**Parameters**	**Accuracy**
Leckie et al. (2003)	8.5cm	2/m^{-2}	tree crown isolation	80% - 90%
Heinzel et al. (2008)	25 cm	7/m^{-2}	tree species classification	83%
Chen et al. (2012)	10 cm	1.7/m^{-2}	Forest canopy modeling	88%
St-Onge & Achaichia (2001)	85 cm	1/m^{-2}	Forest canopy height	90%
Bohlin et al. (2012)	12 cm	7/m^{-2}	Forest variable estimation	Height (92%), Stem volume (86%), Basal area (85%)
Kim et al. (2010)	25 cm	5-10/m^{-2}	Carbon estimation	

1.1.4 Rationale and Problem statement

The assessment of forest above-ground biomass is important for the estimation of long-term carbon storage and for forest resource management (Waring & Schlesinger, 1985). DBH and tree height has been an important parameter used for calculating biomass, which traditionally is estimated by field surveys. However, measuring tree height and biomass estimation by field survey involves very labor-intensive and time consuming work (Kwak et al., 2007). Remote sensing techniques such as aerial photography, satellite imagery and airborne LiDAR data solved the problem of biomass estimation over large areas. The relationship between DBH, tree height and Canopy Projection Area (CPA) should be established from regression analysis to estimate AGB from RS techniques (Popescu & Wynne, 2004). Several RS based approaches have been developed for biomass and carbon estimation. However, most of the existing methods have considerable uncertainties and, thus accurate methods are required (Köhl et al., 2009). In this context, LiDAR data and photogrammetric matching of aerial images can be used to improve the accuracy of estimation of carbon stock compared to other approaches. Airborne LiDAR and digital photogrammetry are considered to be most precise remote sensing means among others for mapping the height of forest canopies (Lim & Treitz, 2004).

Airborne LiDAR is a promising technology for the assessment of AGB but it is difficult to estimate the tree species and tree density in LiDAR data with low point density (Means, 2000). Also, the LiDAR data acquisition is too costly to be used over large areas (Gibbs et al., 2007) . However, 3D point clouds produced through image matching of high spatial resolution digital aerial images cover a large area and can replace the potential of LiDAR data, reducing some of the costs incurred by expensive LiDAR data acquisition (Leberl et al., 2010). Previous studies found that the canopy surface modeling using digital aerial photogrammetry has similar quality compared to that which is obtained by LiDAR data (Bohlin et al., 2012; Järnstedt et al., 2012). The advantages of image matching and good signal-to-noise ratio of digital photogrammetric cameras lead to the improvement of accuracy, reliability and density of automatic point transfer (Haala et al., 2010).

LiDAR can be used for improving traditional photogrammetric methods, but it has poor textural and spectral information in comparison to digital aerial images. While, aerial photography records the features on the ground in their true appearance, even in a 3D form under stereoscopic vision (Rabben et al., 1960). The tree height obtained from LiDAR is more reliable than photogrammetry, because shade obscures bare soil on aerial images (Hyyppä et al., 2008). This problem is not faced by with high density LiDAR imagery. Despite the differences between two technologies, many authors (Ackermann, 1999; Hollaus et al., 2007; Persson et al., 2002) advised the use of combined data from photogrammetry and laser scanning in order to study different forest attributes. In this study, a high density of LiDAR data with an average of 164 points/m^{-2} and aerial images with an average of 16.4 points/m^{-2} available for the Bois-Noir basin, France will be used to assess forest biomass and carbon stock.

Thus, this study aims to explore the accuracy of the forest structural extraction with its high point density and intended to look into the accuracy levels of these two methods for biomass estimation, which is important for sustainable forest management.

1.1.5 General Objective

To compare point clouds derived from i) 3D photogrammetric matching of aerial images and ii) airborne LiDAR for the estimation of biomass/carbon in the Bois noir forests of Barcelonnette, France.

1.1.6 Specific Objectives

1. To compare the heights of conifer and broad-leaved trees derived from aerial image point clouds with tree heights derived from LiDAR point clouds.

2. To estimate the Crown Projection Area (CPA) of conifer and broad-leaved trees derived from aerial image point clouds and CPA derived from LiDAR point clouds.

3. To estimate total above ground biomass/carbon using point cloud extracted from i) aerial image ii) airborne LiDAR data.

1.1.7 Research Questions

1. How accurately can the heights of individual trees be determined from the CHM obtained from i) aerial image and ii) LiDAR data?

2. How accurately can CPA (m^2) of individual trees be estimated on segmented point clouds derived from i) aerial image and ii) LiDAR data?

3. What is total above-ground biomass / carbon stock estimated using point clouds derived from i) aerial image and ii) LiDAR data?

1.1.8 Research Hypotheses

1. Ha: The tree heights obtained from the CHM of LiDAR data are significantly higher at 95% confidence level than the tree heights obtained from aerial image point cloud.

2. Ha: The CPA obtained from segmented point clouds derived from aerial image is significantly greater at 95% confidence level than the CPA obtained from LiDAR data.

3. Ha: There is a significant difference in estimation of biomass/carbon estimated using aerial image point cloud (aerial height + aerial CPA) and LiDAR point cloud (LiDAR height + LiDAR CPA).

1.1.9 Thesis Outline

Chapter 1 provides the research background with the overview of techniques for biomass and carbon stock estimation. It focuses on point cloud generation from aerial photographs and LiDAR. The research problem along with the research objectives, questions and hypotheses are also described in this chapter.

Chapter 2 briefly describes the study area, material and methods adopted to meet the research objectives.

Chapter 3 presents the results of tree height and tree crown delineation from two main datasets (Aerial image and LiDAR). The relationships among different forests variables are also presented in this chapter.

Chapter 4 focusses on the results and are discussed separately under different headings i.e. CHM preparation, tree crown delineation and its assessment and carbon stock estimation.

Chapter 5 presents the research's conclusion providing answers to research questions and possible recommendations for the future research works.

Chapter 2

2.1 STUDY AREA, MATERIALS AND METHODS

2.1.1 Study Area

The study area is a part of Bois noir catchment situated in the South-eastern part of France in the district of Barcelonnette around latitude 44°25′ 22°87′′N and longitude 6°40′ 22°43′′ E. 'Bois noir' is a French word, and it means 'Black Wood' in English. The Barcelonnette basin lies at an elevation ranging from 1100 to 3000 m asl, (Saez et al., 2012). The area is a steep forested basin in the greater L'Ubaye river valley and about 26 km long (Thiery et al., 2007). The study site is about 1.3 km^2, shown in Figure 4. It is a tourist hotspot, famous for skiing in winter and for biking, hiking, paragliding and rafting in a summer.

Climate

The climate of the study area is characterized by dry and mountainous Mediterranean climate with a strong inter-annual rainfall variability (Saez et al., 2012). The rainfall varies between 400 and 1400 mm (Flageollet et al., 1999). The mean annual temperature is around 7.5° C with 130 frost days per annum (Maquaire et al., 2003).

Geology

The Bois noir basin has an irregular rugged topography with slope gradients ranging from 10° and 70° (Saez et al., 2012; Thiery et al., 2007). Geologically, the northern part of Bois Noir is described by morainic colluvium and autochthonous Callovo-Oxfordian black marls, overlaid by deposits of reworked glacial till (Flageollet et al., 1999). Due to these predisposing geological structure, the area is highly sensitive to weathering and erosion. Outcrops of limestone and sandstone characterize the southern part of Bois Noir.

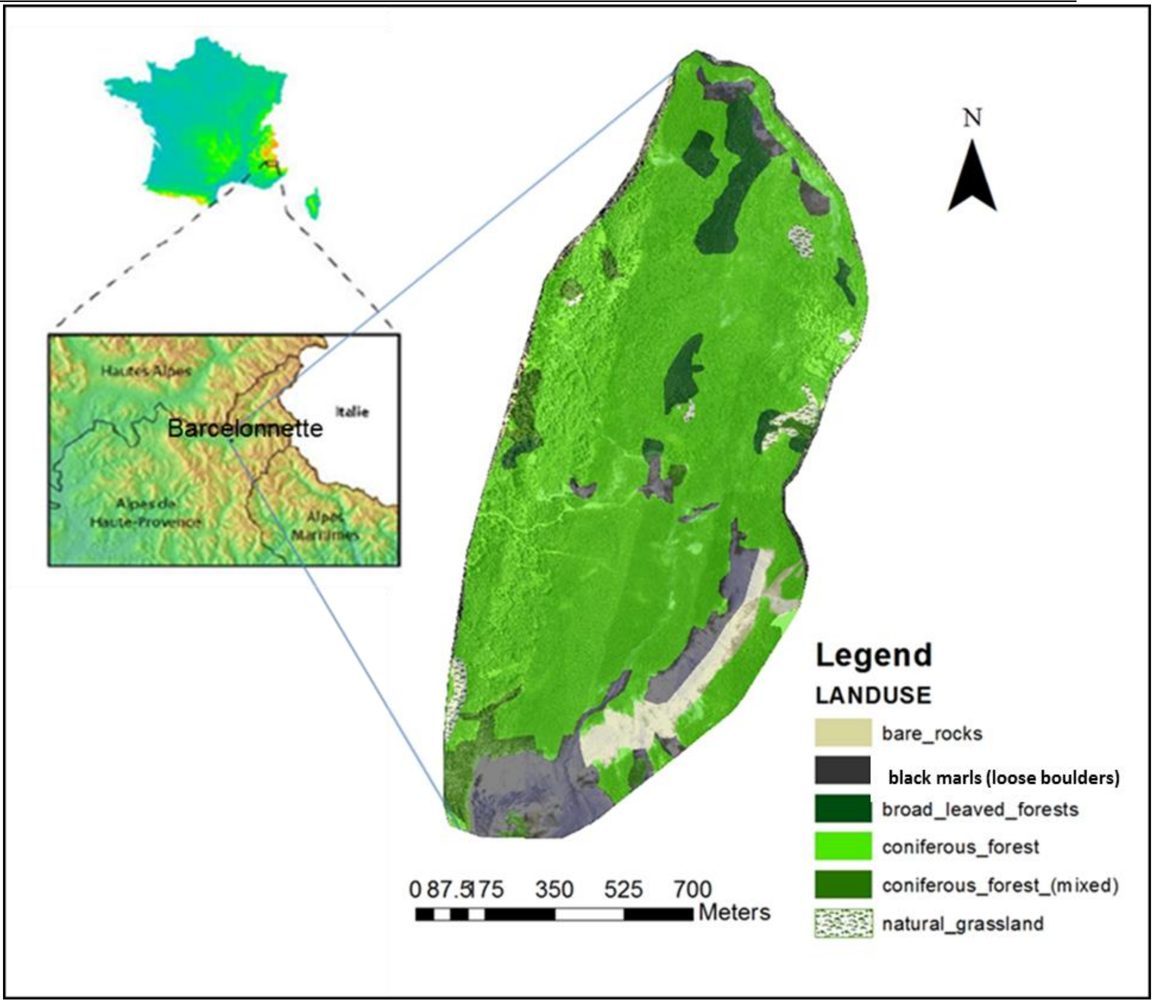

Figure 4: Study area, Bois noir, Barcelonnette, France

Vegetation

About 92% of the total surface area of the Bois noir catchment is covered by forests (Thiery et al., 2007). The Mountain pine (*Pinus uncinata),* Scots pine (*Pinus sylvestris)*, European larch (*Larix deciduas)* and a few Norway spruce (*Picea abies)* are the dominant tree species. Some broadleaved trees such as European beech (*Fagus sylvatica*), ash (*Fraxinus* sp.), alder (*Alnus* sp.), juniper (*Juniperus* sp.), and poplar (*Populus* sp.) were also recorded in the study area during the field work. The forest in the Ubaye Valley was severely degraded by population pressure and soil erosion in the 15th and 16th centuries (Weber, 1994). In the 19th century, reforestation was started over the Ubaye Valley through the enforcement of local laws. A high and frequent landslide activity in the catchment has disrupted the tree stand structures giving rise to so-called "drunken trees" (Razak et al., 2011). A brief description of dominant tree species in the study site is given below:

Pinus sylvestris L.

The Scots pine (*Pinus sylvestris)* is an evergreen coniferous indigenous in the dry inner alpine valleys and the dry Alps. It consists of a single trunk and a rather broad irregular crown. The crown is conical-ovoid in shape with widely spreading to ascending lateral branches. It is readily distinguished from other pines by its combination of fairly short, blue-green leaves and orange-red bark in the upper half of the stem. In the study area, the Scots pines are infested with Mistletoe (*Viscum album* L).

Pinus uncinata Mill. Ex Mirb.

The Mountain pine (*Pinus uncinata*) is naturally found at the tree line in Pyrenees and the Western Alps. It consists of a single trunk, and the crown is conical in shape with narrow spreading lateral branches. The Scots pine and the Mountain pine can be distinguished based on stomata and cuticle characteristics of their needles (Fauvart et al., 2012). A high number of drunken *P. uncinata* trees is found in higher elevations in the study area (Thapa, 2013).

Larix decidua Miller

The European larch (*Larix decidua*) is a deciduous-coniferous tree, native to the mountains of central Europe, in the Alps and Carpathians. The Larch is found at higher elevation in the research area and occurs in small open groups of trees much taller than the surrounding pine trees.

Picea abies L.

The Norway spruce (*Picea abies*) is a fast growing evergreen coniferous tree, native in northern Europe and throughout the Alps. This species is also widely planted outside its natural habitat.

2.1.2 Materials

The airborne LiDAR data and aerial photographs were acquired in July 2009.

Aerial Images

The aerial photographs of 15 cm resolution were co-captured with the LiDAR data (Figure 5). The images were taken by HasselbladH3DII digital camera. A total of 302 images captured and stored in .JPEG file format. The image consists of 3 bands (Red, Green and Blue). The focal length of the camera is 35.026 mm. Detailed specifications are given in Table 2. The ortho image of the study area was prepared from mosaicking aerial photographs and ortho-rectifying in Leica Photogrammetry Suite (LPS) plugin of ERDAS Imagine 10 using LiDAR derived DTM (Kumar, 2012). Aerial image processing resulted into 28,771,790 points, with a mean density of 16.4 points/m^{-2}. The 3D view of study terrain is shown in Figure 6.

Table 2: Metadata for Aerial images

Acquisition date	08.07.2009
Image type	RGB
Flying height	300 m
Scan resolution	0.15 m
Average density	16.4 points/m^{-2}
Image size	49.056 mm x 36.792 mm

Figure 5: Aerial photographs of the study area

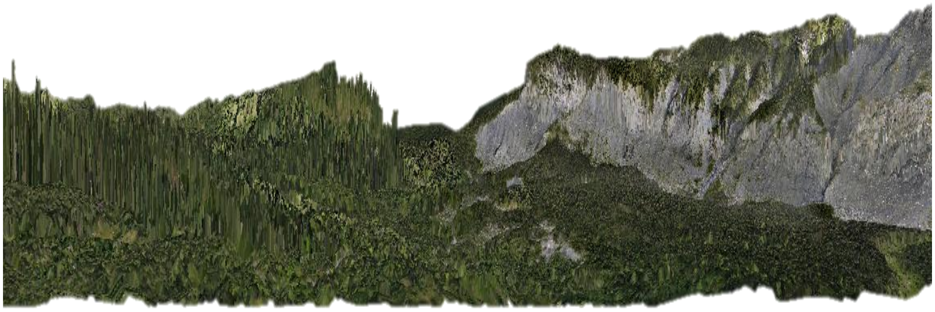

Figure 6: 3D view of photogrammetrically matched aerial images

LiDAR data

A high density airborne LiDAR data was acquired using a helicopter flying at an altitude of 300 m above the ground by Helimap Company SA. A RIEGL VQ-480 laser scanner with a pulse repetition rate of up to 300 kHz was used to record the LiDAR data. The spatial positioning was done using a Topcon Legacy GGD capable of tracking GPS and GLONASS positioning satellites. The orientation of the aircraft was determined using the iMAR FSAS inertial measurement unit (IMU). Seven flight lines were flown at an altitude of 300 m above the ground resulting in 213.7 million points, with a mean density of 164 points/m^{-2} and 113 points/m^{-2} for all and last return records respectively. The LiDAR fight data as obtained from the field was first pre-processed by the vendor using Terrascan software. The point data (X, Y, Z) was produced in LAS1.2 format which contains (X, Y, Z) coordinates, intensity, return number, scan direction, scan angle rank, point source ID, classification and GPS time. In total 17 subsets were provided for the study area in LAS file format. Details of the LiDAR acquisition are given in Table 3. A sample visualization of study area is shown in Figure 7.

Table 3: Metadata for Airborne LiDAR data

Acquistion date	08.07.2009
Laser pulse repletion rate	300 kHz
Beam divergence	0.3 mrad
Laser beam footprint	75 mm at 250 m
Flying height	300 m
Field of view	60°
Average density	164 points m^{-2}
Scanning method	Rotating multi-facet mirror

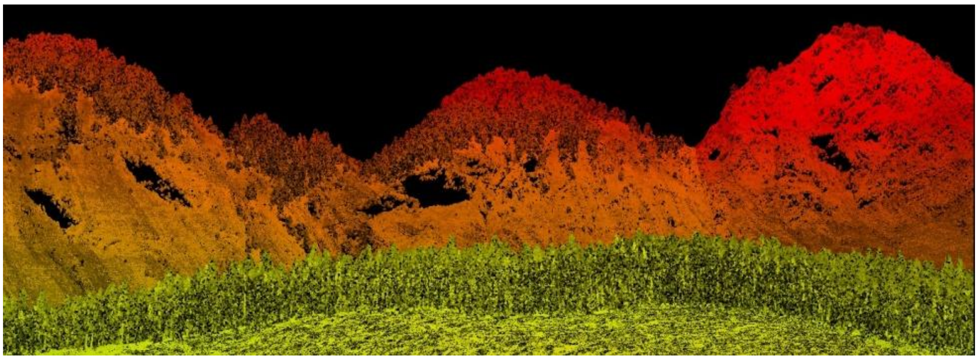

Figure 7: 3D view of LiDAR point cloud (Kumar, 2012)

2.1.3 Methods

The overall method consists of four major parts: field work data collection, aerial photographs and LiDAR processing, object based segmentation analysis and model development. The aerial images were processed to obtain point clouds data and DSM. DSM, DTM and normalised point cloud were generated from processing of liDAR data. Canopy Height Model (CHM) was generated from both datasets and was used to extract height of the individual tree. Individual tree crown delineation was done using Region growing in eCognition software. Accuracy assessment of segmentation was performed. Multiple regression model for both datasets were developed using CPA and height as explanatory variables for carbon estimation. A flow diagram showing the research method is illustrated in Figure 8.

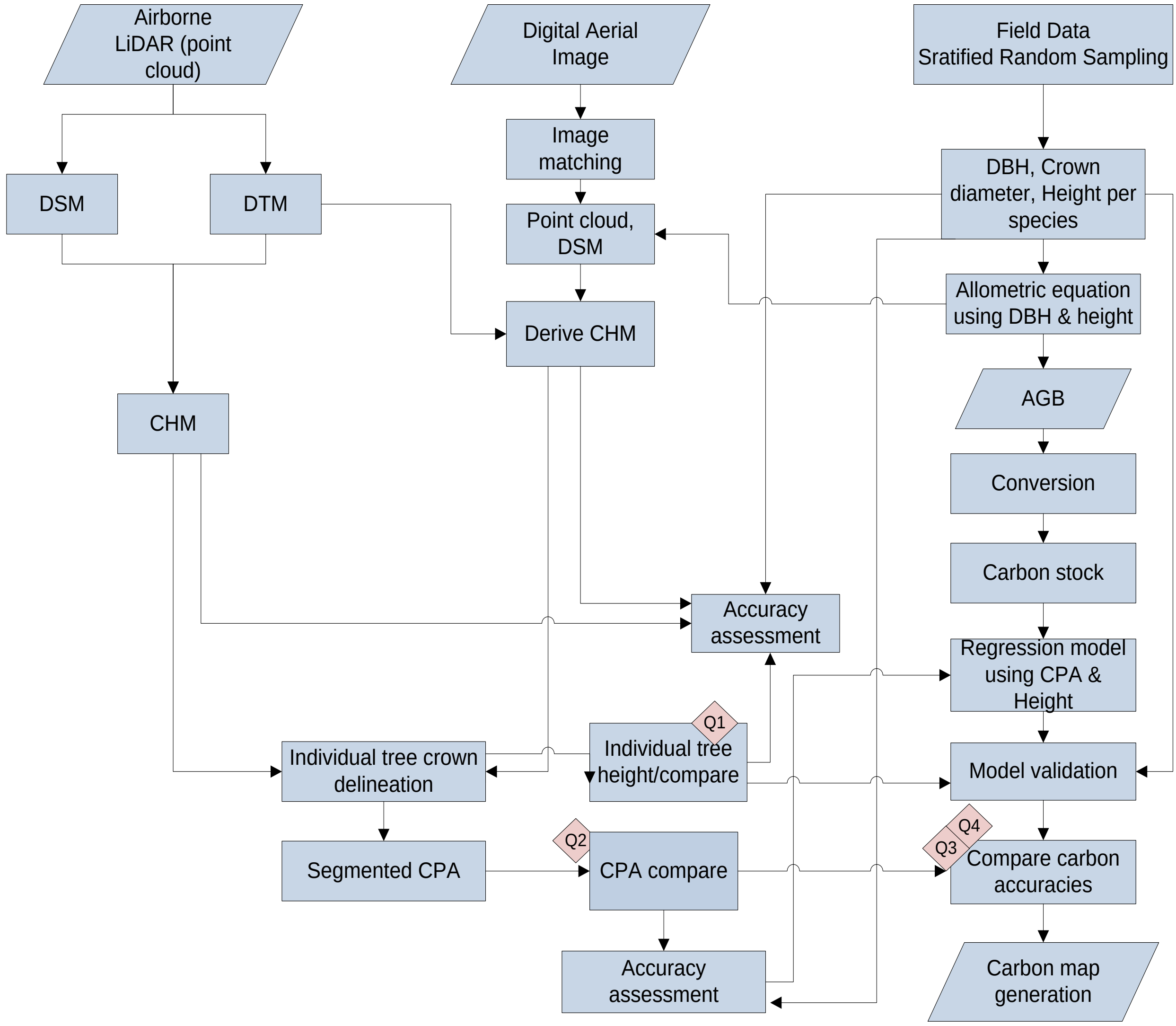

Figure 8: Flowchart of research methods

2.1.3.1 Field Sampling design

A stratified random sampling design based on plots was applied for this study. This sampling design helps to ensure that the sample is spread out over the entire study area and gives more precise estimates of the population parameters of interest (mean or total) (Shiver & Borders, 1996). Stratification was done using a land cover map obtained from the French Forest Service, which was divided into five strata (*i.e,* Scots pine, Mountain pine, broad leaved, mixed forest and bare rock (Office National des Forest, 2000). Twenty-eight plots were visited and measured for this phase, but ancillary data collected in 2011 and 2012 using the same sampling design provided extra sampling plots for this research. Altogether 88 plots were taken into consideration for the study (Appendix 1).

2.1.3.2 Field data collection

Field data collection was carried out during the month of September 2013. A Garmin GPS receiver and orthophoto map were used to locate the center of each plot. A circular plot of 500 m^2 area with a 12.62 m radius was chosen out for the measurement of tree parameters after slope correction (Husch et al., 2003). The Suunto clinometer was used to measure the slope, and the slope correction was performed for all plots having slope larger than five degrees using a slope correction table (Appendix 2). Within the circular plot, trees with DBH 10 cm or greater were measured with DBH tape at height of 1.3 m above the ground. Individual tree height was measured using Haga hypsometer and plot canopy cover was measured using a spherical densiometer from five different locations within the plot and canopy cover was averaged. A total of 28 plots were surveyed. Ancillary data collected in 2011 and 2012 along with the current study provided additional 975 individual trees of known location.

2.1.3.3 Data Analysis

The collected field data was entered appropriately in an Excel sheet. Box plots were made for depiction of collected field data for major tree species. Identified trees on the image during the fieldwork were delineated using ArcGIS. The identified trees were used for developing and validation of the regression model.

2.1.3.4 LiDAR pre-processing

LiDAR data is in the form of discreet point clouds of ground features having X, Y, Z coordinates of all the points where the Z value characterizes the elevation of each point. LiDAR point cloud was obtained in the las format which consists of 17 tiles for the study area. LAStools was used for pre-processing of raw LiDAR data which is the efficient tool and can be used for filtering, tiling, rasterizing, triangulating, converting, clipping, quality-checking etc. (Rapidlasso, 2013). LiDAR pre-processing involved the generation of the Digital Terrain Model (DTM), Digital Surface Model (DSM) and Canopy Height Model (CHM).

DSM, DTM and CHM generation

The Digital Terrain Model (DTM), Digital Surface Model (DSM) and Canopy Height Model (CHM) were generated using LAStools software.

Digital Terrain Models are digital representations of variables relating to a topographic surface, such as elevation (DEM), aspect, gradient, horizontal/vertical land surface curvature and other topographic attributes (Florinsky, 1998). LiDAR DTMs are created by interpolation of ground returns with the assumption that terrain does not change abruptly but gradually (McCullagh, 1988). In total, 9.4 million returns in the point cloud were classified as ground returns. LASgrid tool was used to generate the DTM using ground returns only and a fill of 2 pixels with grid size 0.15 m. The fill function determines the number of pixels to be considered in the prediction of 'no data' pixels based on the neighbourhood during rasterization.

A Digital Surface Model (DSM) represents the earth's surface and includes all objects on it whereas DTM represents the bare ground surface (Heritage & Large, 2009). A DSM is generated from the first canopy return of the LiDAR pulse and LASgrid tool for Windows was used to generate the DSM using the same algorithm as used in DTM generation keeping the highest elevation of first returns.

A Canopy height Model (CHM) or the normalized DSM represents the absolute height of all above-ground features. A CHM was obtained through gridding normalized point cloud using LASheight tool for Windows provided in the LAStools software, keeping the highest elevation of first returns and a 2 pixel fill. Alternatively, it could also be obtained by computing the difference between DSM and DTM using a raster calculator in ArcGIS. The generated CHM showed some noise resulting in high variation in height values of trees which are not true in reality. Thus, we dropped all the noise points and kept the value of CHM as 0 and 40 m.

2.1.3.5 Aerial Images Pre-processing

There are several commercial software and algorithms for the generation of DTM and DSM; point clouds and orthophoto such as Socet set, Match-T DSM, Photosynth and LPS software (Bohlin et al., 2012; Lemaire, 2008). Pix4D software was used in this study which converts thousands of aerial images into geo-referenced 2D mosaics and 3D surface models and point clouds (pix4d, 2014). It is a digital photogrammetric workstation which is fully automated and requires no manual interaction, capable of computing the photogrammetric products: 3D point cloud, DSM and orthophoto mosaic (Naumann et al., 2013). The software searches for and matches points by analysing all uploaded images using a computer vision technique, the SIFT (Scale Invariant Feature Transform) (Lowe, 2004). SIFT identifies the features in images invariant to scaling, rotation, illumination and deformation. This method automatically identifies key-points in each image followed by extraction of vector feature descriptors surrounding the key-points that are invariant of orientation (Lowe, 2004). Those matching points and approximate locations of the cameras are then used in a bundle block adjustment to reconstruct the position and orientation of the camera for every require image (Triggs et al., 2000).

Bundle block adjustment

Bundle block adjustment involves orientation of the entire block of images. It estimates the 3D location of each point corresponds to the location and orientation of cameras (Snavely et al., 2008). The orientation parameters of aerial images are interior and exterior orientation. Pix4D allows computing the block orientation in a fully automatic way, requiring only camera calibration parameters and image geo-location as an input (Gini et al., 2012). Ground Control Points (GCPs) were included together with corresponding image points within bundle block adjustment to improve spatial accuracy (Naumann et al., 2013). Bundle block adjustment refines the structure from motion by non-linear least square solution minimizing the reprojection error (Lourakis & Argyros, 2009).

Dense Image matching

Pix4D performs abovementioned tasks as part of an automated computer vision SfM (Structure from Motion) pipeline in order to produce 3D RGB point cloud (Verhoeven, 2011). Dense image matching is used to match a huge number of pixels automatically to generate a surface model from a set of overlapping digital images. The matched points after bundle block adjustment can have their calculated 3-D coordinates. Those 3D points are interpolated to form a triangulated irregular network to achieve a mesh Digital Surface Model (DSM) through image matching (Küng et al., 2011). The quality of images, orientation, and camera calibration determine the quality of DSM. The geometry accuracy of DSM from image matching depends upon the image correction coordinated from bundle block adjustment (Haala, 2009). Figure 9 depicts the entire processing pipeline in generating 3D point cloud.

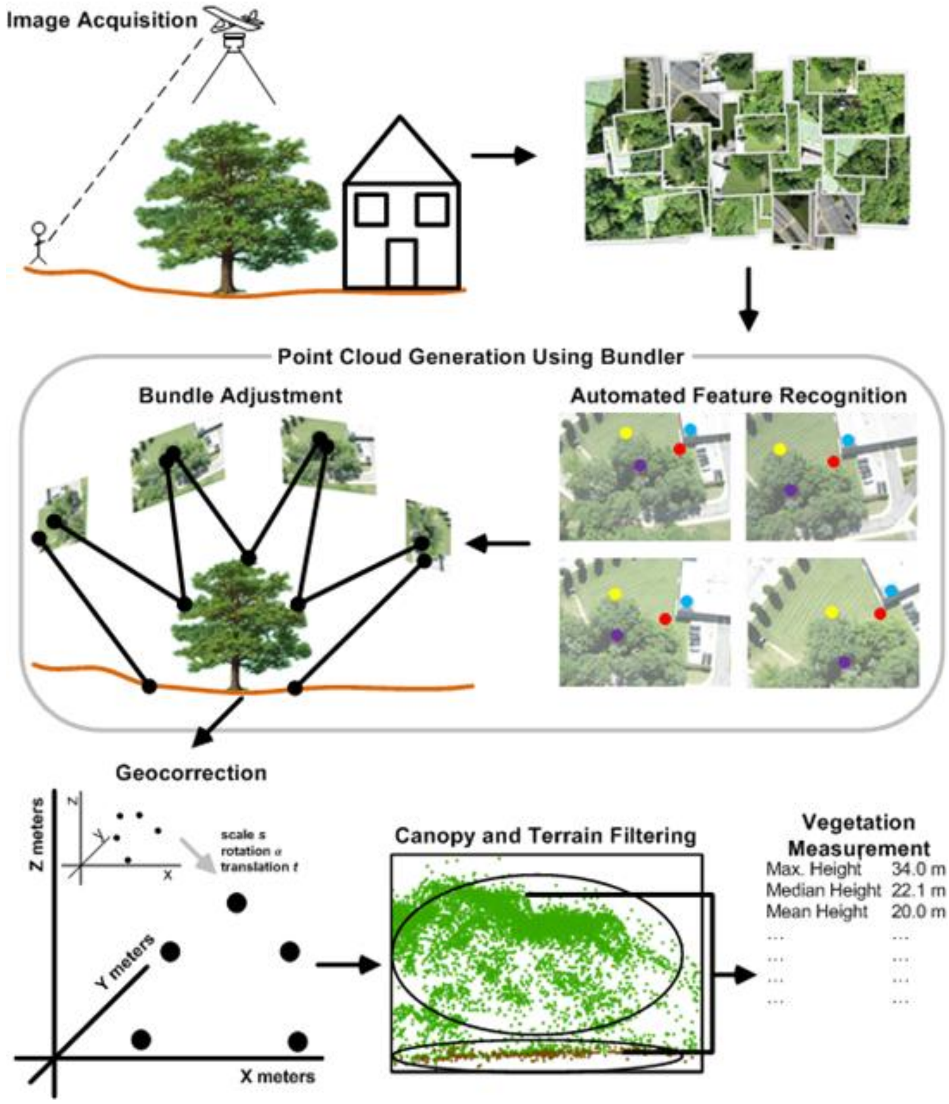

Figure 9: 3D point cloud generation by building geometry form matching features identified in multiple overlapping photographs (Dandois & Ellis, 2013)

CHM generation

The aerial photo CHM was generated by subtracting the LiDAR DTM from the Aerial DSM. The point clouds of the aerial image have one return, and therefore they cannot estimate the ground level of terrain properly. Thus, the point cloud generated from the aerial image only contains DSM. LiDAR DTM performed better than aerial photo DTM as LiDAR has multiple returns. DTM can be constant for a long time, but DSM needs to be accurate and up-to-date to get CHM. Thus, (Schardt et al., 2004) suggest using DTM from LiDAR to achieve better accuracy for forestry purposes. The co-registration of LiDAR DTM was done with Aerial DSM which resulted with root mean square error (RMSE) of 0.29 m (Appendix 3). Matching of different sources of information can be sometimes impossible due to terrain slope and tree height (Valbuena et al., 2008). Thus, error introduced during the co-registration process subsequently leads to the error in segmentation and height extraction.

2.1.3.6 Validation of CHM

The LiDAR derived tree height and photogrammetrically derived tree height were compared to the corresponding height of the corresponding field measured tree. The LiDAR and photogrammetrically derived tree height were extracted as a maximum pixel value from CPA of the CHM. The tree height derived from point clouds of LiDAR and Aerial image were regressed against field height, which yielded a R^2 to validate the CHM created. Pearson's correlation test and one - way ANOVA test were carried out to find out if there is a significant difference between their heights.

2.1.3.7 Tree crown delineation

Segmentation of individual trees and extraction of relevant tree structure information from remotely sensed data is very useful in forestry (Chen et al., 2006). For a delineation of tree crown, the crowns should be recognizable as a distinct object in the remote sensing images and the spatial resolution of the image should be much higher than the tree crown size. Segmenting an image into meaningful objects is an initial step of object based image analysis (OBIA) which involves grouping neighbouring pixels into significant image objects (segments) based on homogeneity criteria. Several methods exist for segmentation of the image depending on the algorithms having different characteristics. Some of the commonly used algorithms include watershed segmentation (Wang et al., 2004), region growing (Ke & Quackenbush, 2008), valley following (Gougeon & Leckie, 2006), multi-resolution (Yu et al., 2006). The segmentation techniques can be grouped into top-down and bottom-up approach. Top down approach includes cutting big objects into smaller pieces through Chessboard, Quadtree, Contrast filter and Contrast split segmentation while bottom up approach is merging of small pieces so as to get bigger objects based on homogeneity criteria (Karna, 2012). In this study, chessboard segmentation and the region growing method were used in eCognition Developer 8.7 software to derive the tree crowns. The image segmentation process was as follow:

Smoothening/Filtering

Both the orthophoto and LiDAR CHM were smoothened to improve an image visual interpretability and to avoid the finding of false tree tops within a tree

(Reitberger et al., 2007). This was done by applying a Convolution filter, which replaces each pixel value by the average of the square of the matrix centred on the pixel (eCognition, 2011). In this study, 3 X 3 kernel size was used for the filtering.

Chessboard segmentation

Chessboard segmentation is a top-down segmentation strategy in which an image objects split into smaller objects into equal squares of a given size (Definiens, 2007). The object size is the most important parameter in chessboard segmentation, which has to be specified by the user. Grid size of 2*2 pixels was used for chessboard segmentation based on processing capability of eCognition. Figure 10 illustrates the chessboard segmentation having square grid of fixed size aggregated into meaningful objects. After chessboard segmentation, the resulting objects were divided into two preliminary classes: tree and others. The mean brightness value from the aerial image and height information from LiDAR CHM were used to assign the classes. Objects (tree) with height less than 2 m were removed (Næsset, 1997) in order to have trees with significant stem volume for biomass calculation.

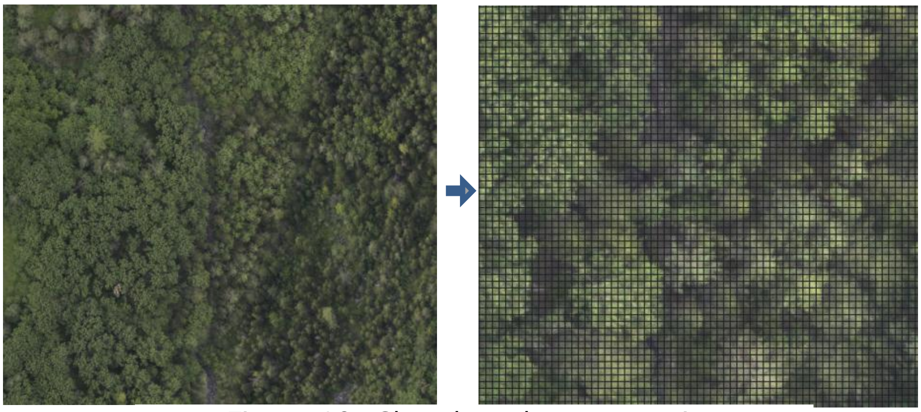

Figure 10: Chessboard segmentation

Region Growing Approach

Region Growing is bottom-up segmentation where the segments grow, according to some similarity rules, from a number of seed points. It starts with one pixel objects and subsequently merges pairs of adjacent objects into larger objects based on the smallest growth of heterogeneity, which may be defined through spectral variance and geometry of object (Definiens, 2007). This approach needs seed points to be specified first. Starting at potential seed pixels, neighbouring pixels are examined and added to growing region if they are similar to the seed pixels (Ke & Quackenbush, 2008). Individual tree segmentation was done using local maxima (peaks) and local minima (valleys). Local maxima are used a seed points to grow into meaningful objects and it looks like peak of the mountain and local minima are used as a restriction for growing region which looks like valley (Culvenor, 2002) (Figure 11). The algorithm assumes that the centre of the crown is brighter than the edges (Culvenor, 2002).

The CHM and orthophoto were used as primary raster layers for Region Growing segmentation. Tree crown delineation was done based on growing of treetop using local maxima and local minima to define likely crown boundaries. Treetop detection can vary with window size; thus, an appropriate window size or threshold should be chosen. In this study, a 5x5 window size was chosen to fit the average crown diameter of 2.9 meters measured in the field.

Firstly, local minima were identified defining the "search range window" size and local minima that were close to each other were merged as they form the edge of the segmented object or the boundary of the tree crown. Then, local maxima were identified but all identified tree tops were not true tree tops as the algorithm identified more than one tree top for a single tree. To remove false tree tops, all tree tops which neighbours to one another were merged. Then region growing from tree top was started until it reached the local minima. Minima were used to control the relative growth of crown so as to prevent neighbouring crowns intruding each other's space (Kumar, 2012). Tree crowns were grown in relation with neighbouring objects. Local maxima and local minima were identified using height information from the CHM and extracted using "find enclose by image object" (Kwak et al., 2007).

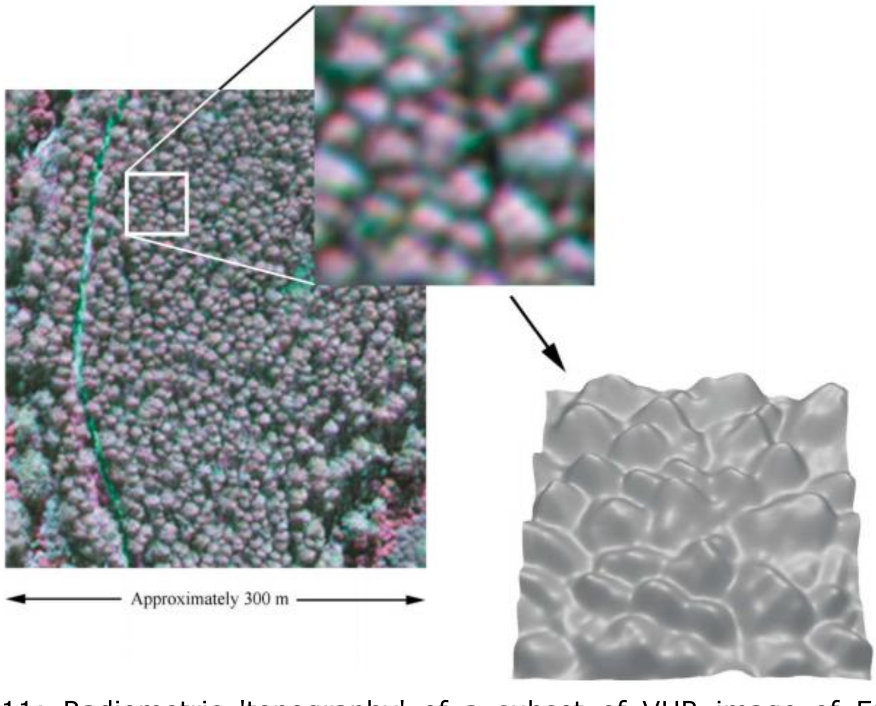

Figure 11: Radiometric 'topography' of a subset of VHR image of Eucalypt forest (Culvenor, 2002)

2.1.3.8 Accuracy assessment of tree crown delineation

Segmentation validation is related to quality of data (noise, spatial and spectral resolution) and the optimal customization of parameter settings (Möller et al., 2007). There are several methods for segmentation validation. In this study, validation of the segmentation was done using two accuracy measures i.e. Relative Area measures developed by (Clinton et al., 2010) and 1:1 correspondence (Zhan et al., 2005).

Clinton et al. (2010) have developed a geometrical segmentation accuracy measures in terms of over and under segmentation; and goodness of fit (D). Over segmentation and under segmentation as defined by (Clinton et al., 2010) are given in equations 1 and 2.

$$Over\ segmentation_{ij} = 1 - \frac{area\ (Xi \cap Yj)}{area\ (Xi)} \ \ldots\ldots\ldots\ldots\ldots\ldots\ldots 1$$

$$Under\ segmentation_{ij} = 1 - \frac{area\ (Xi \cap Yj)}{area\ (Yj)} \ \ldots\ldots\ldots\ldots\ldots\ldots\ldots 2$$

Where *xi* is a reference object and *yj* is a corresponding segmented objects.

The value of over segmentation and under segmentation lies within the range of 0 to 1, where 0 value means a perfect segmentation (Clinton et al., 2010). The segmentation goodness or closeness of fit (D) is a measure of error in segmentation (equation 3). The D value ranges from 0 to 1 and a D value equals to 0 means perfect segmentation (Clinton et al., 2010).

$$D = \sqrt{\frac{over\ segmenation^2 + under\ segmenation^2}{2}} \ \ldots\ldots\ldots\ldots\ldots 3$$

1:1 spatial correspondence was assessed by matching manually delineated tree crowns with automated segments. A higher percentage of 1:1 correspondence indicates a higher accuracy.

2.1.3.9 Above Ground Biomass and Carbon Stock calculation

For the estimation of above-ground biomass (AGB), a crucial step is to determine the allometric equations which can be used to estimate carbon stock of forests. Site specific allometric equations were not available for the tree species recorded in the study area. The following allometric biomass equations of *Pinus uncinata* (Spain), *Pinus sylvestris* (Italy), *Larix decidua* (Italy) and *Fagus sylvatica* (Italy) were used for the carbon estimation in the study area. The allometric equations for these tree species were available from an international web platform, GlobAllomeTree. This platform support volume, biomass and carbon stock assessment (GlobAllomeTree, 2013). The equation for each tree species is given in equations 4 to 8 below:

P.uncinata
AGB = 0.0203*DBH^2*H……………………………………………………………………4
P.sylvestris
AGB = DBH^1.82075*H^1.07427*exp(-2.8885)……………………………..5
L. decidua
AGB = 8.8267+0.03426*DBH^2*H+0.27518*DBh^2……………………..6
F. sylvatica
AGB = 0.03638*DBH^2.15436*H^0.6587……………………………………….7

Where,

AGB = above ground biomass (kg)
DBH = tree diameter at breast height (cm)
H = tree height (m)
Exp = exponential function

Furthermore, carbon stock of the tree species was calculated from AGB using a conversion factor of 0.47 (about 47% of the dry biomass is assumed to be carbon for all parts of trees as a default value) as suggested by IPCC (2006).

Carbon stock = 0.47 × AGB………………………………………….8

2.1.3.10 Regression analysis and model validation

Regression analysis has been intensively used for modelling the relationship between response variable and one or more explanatory variables. The analysis provides quantitative relationship and is expressed by an equation and its graphic representation (Husch et al., 2003). The coefficient of determination (R^2) and root mean squared error (RMSE) help to evaluate the model performance. Generally, a higher R^2 or a lower RMSE value indicates a good fit between observed and predicted outcomes (Lu, 2006). R^2 gives the proportion of the variance of one variable that is predictable from the other variable. RMSE gives error in kg which is calculated as follows:

$$RMSE = \sqrt{\frac{1}{n}\sum_{i=1}^{n}(X_{O\mathrm{i}} - X_{P\mathrm{i}})^2} \qquad \text{……………………………9}$$

Where,
Xo = Observed carbon
Xp = Predicted carbon
n = Number of observation

In this study, AGB considered as a dependent variable while other variables such as segmented CPA (LiDAR CPA and aerial CPA) of each tree and the height derived from LiDAR and aerial derived height were considered as independent variables. In order to avoid multi-collinearity amongst the explanatory variables (CPA and height), the Variation Inflation Factor (VIF) was calculated. A VIF value above 10 indicates the effect of multi-collinearity on the model (O'brien, 2007).

The individual tree which had 1:1 spatial correspondence with reference and delineated tree crowns were used for model development and validation since incorrectly identified and misclassified trees cannot be used for evaluation (Pouliot et al., 2002). Besides this, outliers should also be removed to establish a robust model. Therefore, the total number of observations become less than that of the number of trees that were initially identified on the image. Validation of the model was carried out using 30% of the field measured data to determine the significance and strength of the relationships.

2.1.3.11 Estimation of AGB and Carbon stock

After the regression model was developed and validated, the model was applied to estimate AGB and carbon stock in the study area. The CPA and height derived from aerial point clouds and CPA and height derived from LiDAR data were used as independent variables to produce estimates of AGB and carbon stock. A carbon map of the study area was prepared using ArcGIS.

Chapter 3

3.1 RESULTS

3.1.1 Descriptive analysis of field data

Forest stand parameters (DBH, height and crown diameter) were recorded from 88 sampling plots in the study area. In total, DBH was measured for 2180 trees while the height and crown diameter of 1377 and 892 trees were measured respectively. Descriptive statistics of sampled data are shown in Table 4.

Table 4: Descriptive statistics of sampled trees

Statistics	DBH (cm)	Height (m)	Crown diameter (m)
Mean	21.75	13.25	3.08
Minimum	10	5.20	0.50
Maximum	61	29	11.10
Standard Deviation	8.26	3.52	1.55
Number of trees	2180	1377	892

Bois noir is dominated by conifer species. *Pinus sylvestris* and *Pinus uncinata* are the dominant species with occurrence of 48% and 41% respectively. Other tree species are *Fagus sylvatica*, *Larix decidua*, *Fraxinus excelsior* and *Picea abies*. Details of occurrence of these tree species as observed during the field study are given in Figure 12.

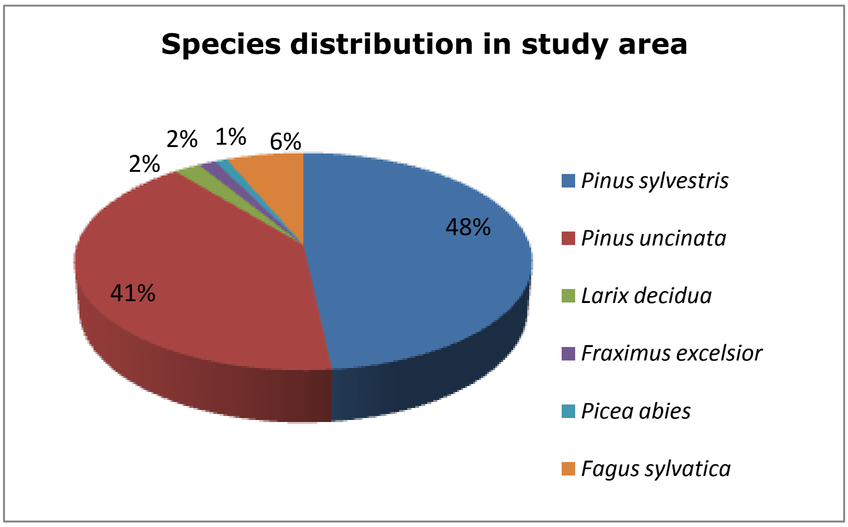

Figure 12: Species composition of study area

DBH, height and crown width of dominant tree species were analysed and presented by Box-plots which are given in Figures 13 (a,b,c). *Larix decidua* has the largest DBH and *Pinus uncinata* has the smallest DBH on average. In case of mean height, *Fagus sylvatica* is found to have highest height followed by *Larix decidua*, *Pinus sylvestris* and *Pinus uncinata*. Similarly, *Larix decidua* is found to have largest crown diameter. All tree attributes of these tree species show a normal distribution (Appendix 4).

a. Box plot of DBH

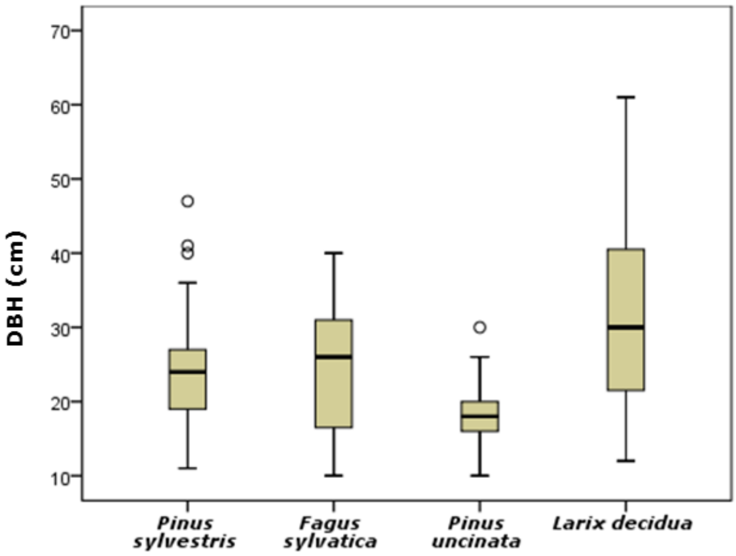

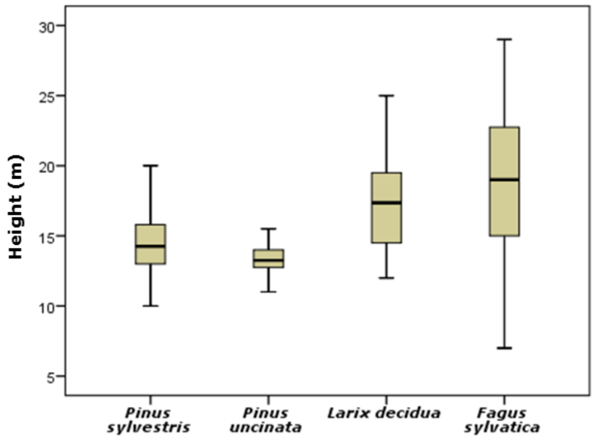

b. Box plot of height

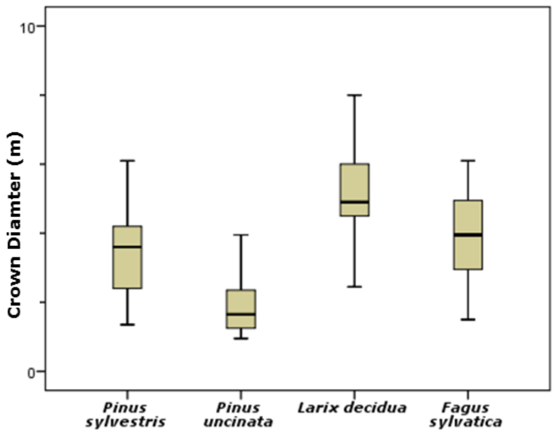

c. Box plot of crown diameter

Figure 13: Box plot of DBH, height and crown diameter of major tree species

3.1.2 CHM generation from LiDAR data

LiDAR data was processed to obtain the canopy height model (CHM) as shown in Figure 14. The extracted ground points were interpolated for generating a DTM while the first return points were interpolated for generating a DSM which are shown in Figure 14 (Top Left, DSM, Top Right, DTM). Figure 14 (Bottom) shows the CHM, which was created by subtracting DTM from DSM.

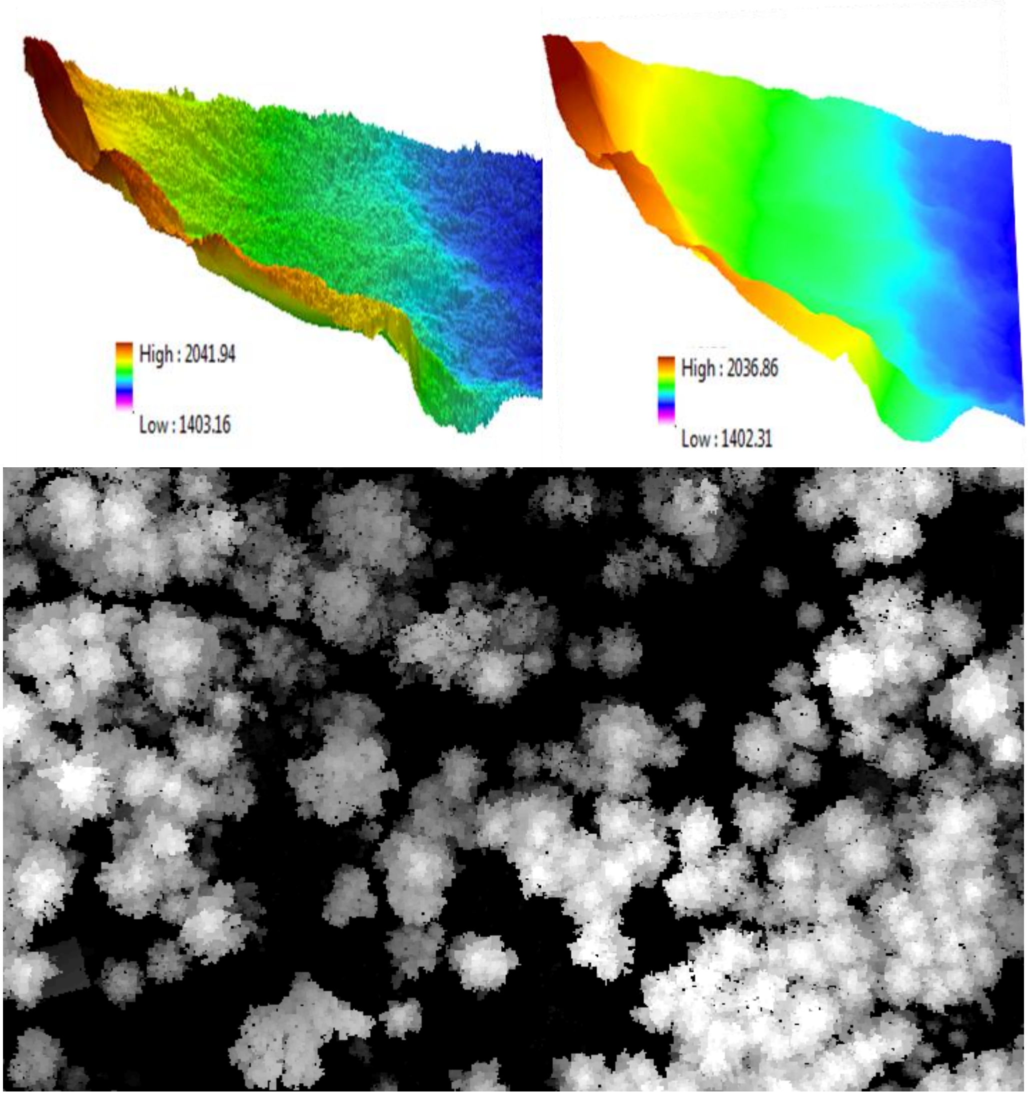

Figure 14: LiDAR derived images (Top Left, DSM, Top Right, DTM and Bottom: CHM)

3.1.3 Assessment of LiDAR derived tree height

A total of 340 tree heights measured in the field with a Haga hypsometer and corresponding heights extracted from LiDAR were used as a sample dataset. Summary statistics for both height performances showed that the average mean value of LiDAR derived height was 0.10 m lower than the field height. A linear regression between the LiDAR derived height and field measured height (Figure

15) showed R^2 values of 0.813 and RMSE of 1.18. Summary of statistics for both height performances is given in Table 5.

Table 5: Summary of statistics for LiDAR and field height measurements

Statistic	**Field height(m)**	**LiDAR derived height (m)**
Mean	11.88	11.78
Minimum	5.20	5.08
Maximum	25	23.66
Std Deviation	2.56	2.72
Observations	340	340

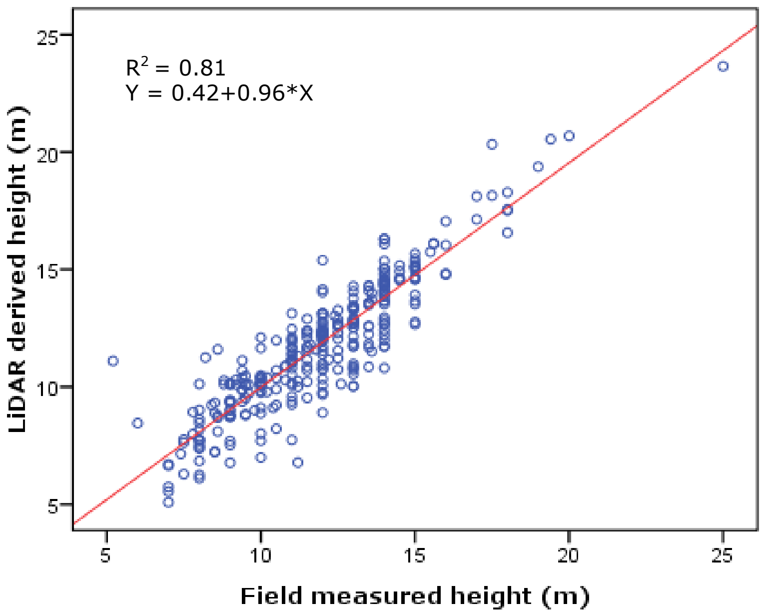

Figure 15: LiDAR derived tree height compared with Field measured height

3.1.4 CHM generation from Photogrammetric matching of Aerial Images

The canopy height model (CHM) was generated from the aerial point clouds. To come up with a CHM, a DSM was created by interpolating the single returns of the aerial images. For the DTM, the LiDAR DTM was used. The subtraction of LiDAR DTM from aerial DSM represents the absolute height of trees in the study area. Figure 16 shows the CHM (Bottom), which was obtained by subtracting DTM (Top, Right) from DSM (Top, Left).

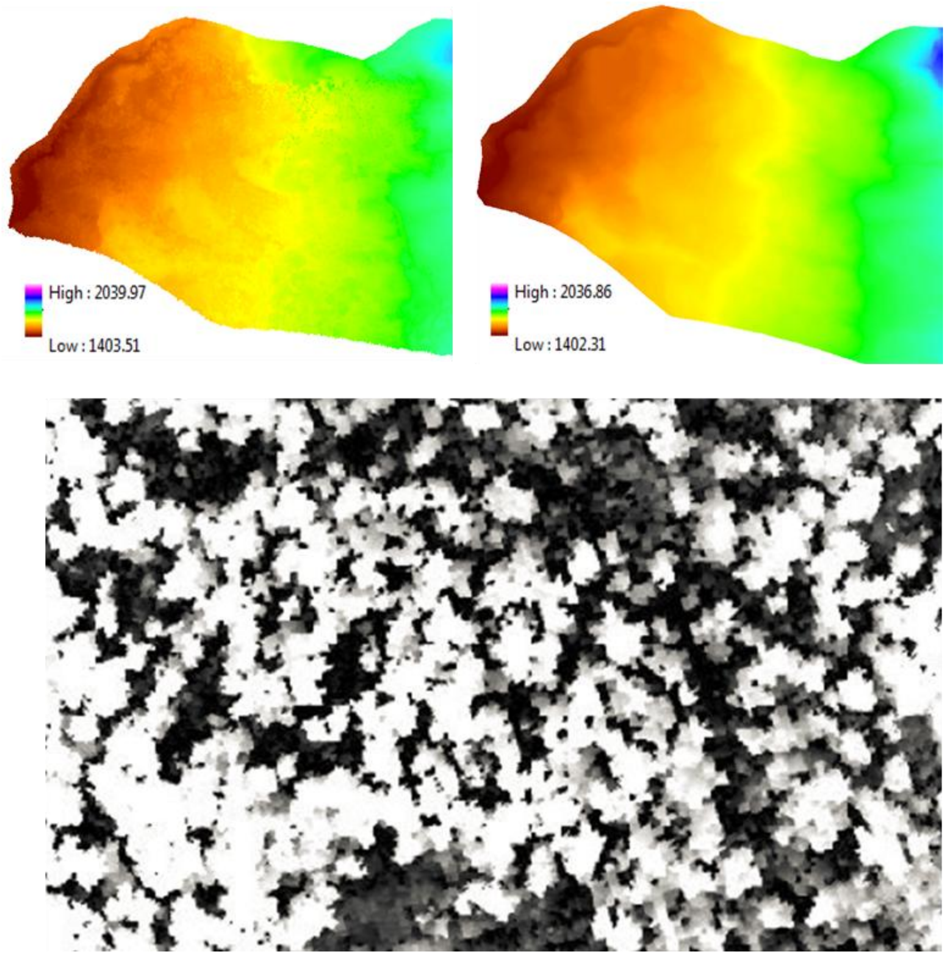

Figure 16: Illustration of DSM (Top, Left), DTM (Top, Right) and CHM (Bottom) for a part of the study area

3.1.5 Assessment of tree height derived from Aerial Images

Tree height derived from Aerial Image was compared with the field measured height using linear regression model as shown in Figure 17. This was done using 340 observations. The coefficient of determination (R^2) was 0.66 and an RMSE of 1.69 was obtained. The aerial derived height was underestimated by 0.66 m on average. Summary of statistics for both height performances is given in Table 6.

Table 6: Summary of statistics for tree height measurements

Statistic	Field height (m)	Aerial derived height (m)
Mean	11.88	11.22
Minimum	5.20	5.67
Maximum	25	22.88
Std Deviation	2.56	2.57
Observation	340	340

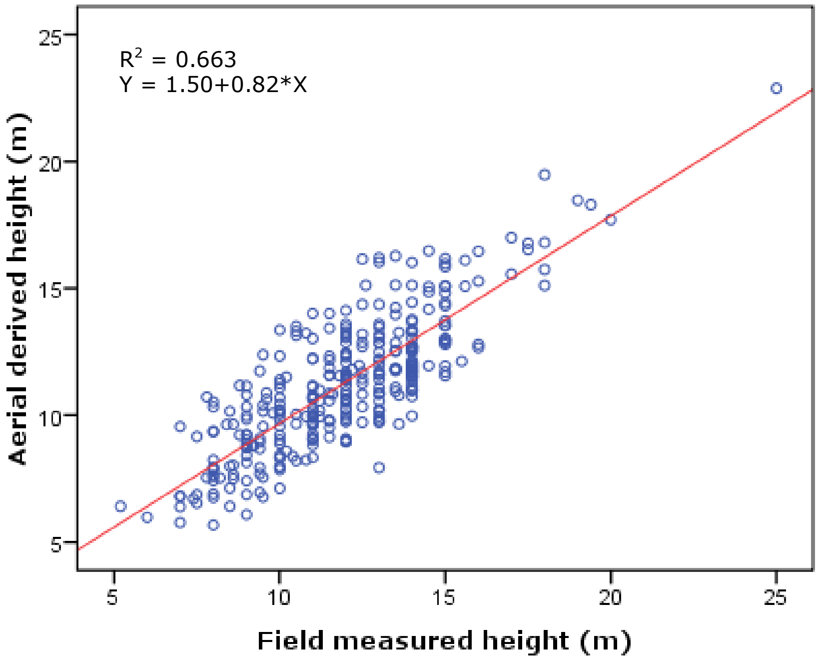

Figure 17: Scatter plot between heights derived from aerial imagery and field measurement

A paired-test was applied to test the hypothesis 1 as shown in Table 7 and it was concluded that there is no significant difference between height measured from field and height derived from LiDAR since the t - statistic is less than t - critical so two means are not statistically significantly different. On the contrary, in the case of Aerial data, the t - statistic is greater than t - critical value so the two means are statistically significantly different. When comparing LiDAR height and Aerial height, F - statistic is greater than F - critical, which indicates that two means are statistically significantly different (Appendix 5). Also the linear regression was performed between ground-measured heights with the LiDAR and Aerial derived heights, which showed a greater R^2 in case of LiDAR derived heights than that of Aerial derived heights. For this reason, LiDAR derived heights are closer to field measured heights.

Table 7: Summary of statistical test

Test / **Paired t-test**	**df**	**t-stat**	**P value**	**t critical**
Aerial	1, 339	7.85526	2.66E-14	1.966986
LiDAR	1, 339	1.55042	0.006099	1.966986

Pearson's correlation (R) and RMSE between field measured tree height and predicted tree height is illustrated in Table 8. The correlation between measured and predicted tree heights of broadleaved trees is greater than that of conifer trees in the case of LiDAR while the correlation of conifer is greater than that of broadleaf trees in case of the aerial images. The tree heights of conifer trees have a smaller RMSE than those of broadleaved trees in both the LiDAR and the aerial images.

Table 8: Goodness-of-fit statistics between field tree heights and those predicted from LiDAR CHM and Aerial CHM

	LiDAR		**Aerial Image**	
Numbers	**Correlation**	**RMSE(m)**	**Correlation**	**RMSE(m)**
Conifer (334)	0.90	1.17	0.81	1.68
Broadleaf (6)	0.93	1.57	0.79	2.40
Total (340)	0.90	1.18	0.81	1.69

3.1.6 Tree crown delineation and accuracy assessment

Individual tree crown delineation was done using the region growing approach. Figure 18 shows the results of delineated individual tree crowns using a subset of aerial image and LiDAR.

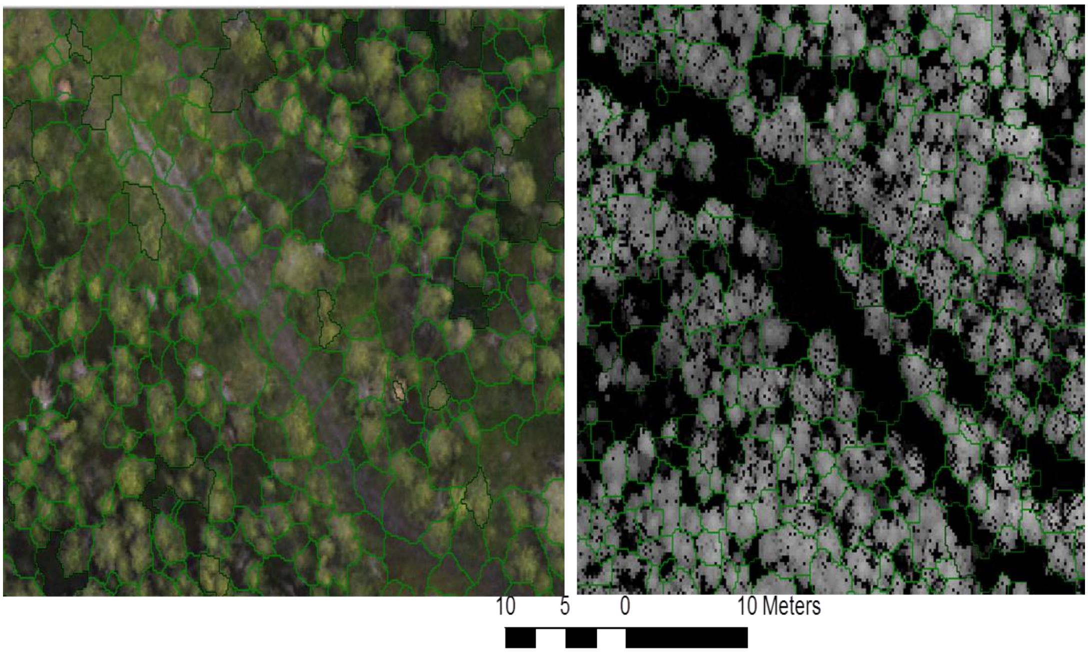

Figure 18: A subset of segmentation results. Left: Aerial Image and Right: LiDAR

The accuracy measures of D and 1:1 spatial correspondence were used for the validation of tree crown segmentation using 277 and 292 manually delineated tree crowns in case of aerial images and LiDAR respectively. The quantitative accuracy assessment with manually delineated crown data showed that the aerial crown delineation was more accurate. Overall, over-segmentation error was 31% and 28% in LiDAR and Aerial image datasets respectively. Similarly, under-segmentation error was 35% and 33% in LiDAR and aerial image datasets respectively. The goodness of fit (D) was 0.33 and 0.30 for LiDAR and aerial images datasets respectively. This means that the total accuracy of tree crown delineation in the case of LiDAR was about 67%, which means 33% of segmentation error. The total accuracy of tree crown delineation in the case of aerial image was 70%, which means 30% of segmentation error.

To assess the accuracy of 1:1 spatial correspondence, the manually delineated tree crowns and the automated segments from the region growing segmentation were compared on a one to one basis. Out of 277 manually delineated reference tree crowns, 221 automated segments had a one to one relationship in case of aerial image dataset (Table 9). Thus, the overall segmentation accuracy was 79.8%. Similarly, out of 292 reference polygons for LiDAR dataset obtained from manual delineation, only 226 automated segments had a one to one relationship as shown in Table 10. Overall, the segmentation accuracy was 77.4%.

Table 9: Matching of 1:1 correspondence of reference polygons to segmented polygons using Aerial Image

Tree species	No. of Reference polygons	1:1 Correspondence	Accuracy (%)
Pinus uncinata	136	109	80.15
Pinus sylvestris	116	94	81.03
Larix decidua	9	8	88.89
Broadleaved trees	16	10	62.50
Total	**277**	**221**	79.78

Table 10: Matching of 1:1 correspondence of reference polygons to segmented polygons using LiDAR

Tree species	No. of Reference polygons	1:1 Correspondence	Accuracy (%)
Pinus uncinata	137	111	81.02
Pinus sylvestris	128	101	78.91
Larix decidua	10	5	50.00
Broadleaved trees	17	9	52.94
Total	**292**	**226**	**77.40**

Figure 19 shows the overlay of the image objects and reference crowns for the 1:1 method of accuracy assessment of segmentation process. The purple objects represent the manually delineated crowns for the identified trees while the red objects are the output of automated segmentation.

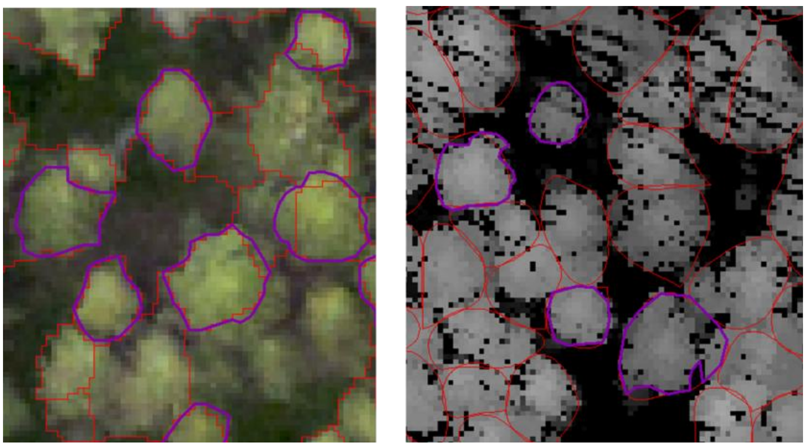

Figure 19: Overlap between the image objects and reference crowns. Left: Aerial Image and Right: LiDAR

3.1.7 Correlation analysis

Pearson's correlation coefficient was calculated to analyse the strength of the linear relationships among the variables such as field measured DBH, segmented CPA from both aerial and LiDAR datasets, CHM derived from aerial point clouds and LiDAR and carbon stock of trees. The relationships among these variables were shown in Table 11 and 12 for four different tree species. 70% of the datasets were used for model calibration and 30% for validation to determine the strength of relationship. Table 11 shows the correlation among the tree variables using aerial image and Table 12 depicts the correlation among the tree variables using LiDAR data.

Table 11: Correlation among the variables of regression model using Aerial Image

Species Name	Variables	df(n-2)	r	R square	P value
Pinus uncinata	DBH and carbon	78	0.91	0.82	< 0.01
	CHM and carbon	78	0.63	0.39	< 0.01
	CPA and carbon	78	0.46	0.21	< 0.01
Pinus sylvestris	DBH and carbon	68	0.91	0.84	< 0.01
	CHM and carbon	68	0.52	0.27	< 0.01
	CPA and carbon	68	0.52	0.27	< 0.01
Fagus sylvatica	DBH and carbon	14	0.79	0.62	< 0.01
	CHM and carbon	14	0.88	0.78	< 0.01
	CPA and carbon	14	0.67	0.45	< 0.01
Larix decidua	DBH and carbon	8	0.99	0.98	< 0.01
	CHM and carbon	8	0.87	0.75	< 0.01
	CPA and carbon	8	0.67	0.45	< 0.01

Table 12: Correlation among the variables of regression model using LiDAR

Species Name	Variables	df(n-2)	r	R square	P value
Pinus uncinata	DBH and carbon	78	0.93	0.87	<0.01
	CHM and carbon	78	0.64	0.41	<0.01
	CPA and carbon	78	0.37	0.14	<0.01
Pinus sylvestris	DBH and carbon	68	0.95	0.91	<0.01
	CHM and carbon	68	0.64	0.41	<0.01
	CPA and carbon	68	0.33	0.11	<0.01
Fagus sylvatica	DBH and carbon	14	0.63	0.39	<0.01
	CHM and carbon	14	0.89	0.79	<0.01
	CPA and carbon	14	0.61	0.37	<0.01
Larix decidua	DBH and carbon	8	0.97	0.95	<0.01
	CHM and carbon	8	0.83	0.69	<0.01
	CPA and carbon	8	0.72	0.52	<0.01

There are strong positive correlations between tree DBH and carbon (>0.70) in almost all of the tree species in both aerial image and LiDAR datasets. The correlation between them are highly significant ($P<0.01$). In general, the correlation coefficient of carbon with CHM and carbon with CPA for both datasets was found to be less than that of carbon with DBH. The correlation coefficient between CPA and carbon is more than 0.60 in the case of *Fagus sylvatica* and *Larix decidua* in both aerial and LiDAR datasets. The lowest r value was found for CPA and carbon of *Pinus sylvestris* in the case of the LiDAR data.

3.1.8 Model calibration and Validation

Multiple regression models were developed for four tree species so as to estimate carbon stock. CPA and height were used as explanatory variable to estimate the carbon stock of individual trees. A linear regression model in Log form was developed for each of the species which describes the relationship between CPA, height and carbon stock. This is shown in equation 10. The relationship among these variables was found to be significant at the 95% confidence level. A collinearity test was done to avoid multicollinearity which may be a problem amongst the explanatory variables (i.e. CPA and height). Variance inflation factor (VIF) was applied for this. VIF was less than 10 for all four species. Summary statistics and regression coefficient of variables for both aerial and LiDAR datasets are presented in Tables 13 and 14. Details of the ANOVA table and other parameter estimates are presented in Appendix 6.

$$\text{Ln Carbon} = \beta_0 + \beta_1 * \text{Ln(CPA)} + \beta_2 * \text{Ln(Height)} \quad \ldots\ldots\ldots 10$$

(Multiple regression model)

Where,

Ln is natural logarithm to the base 2.71828
Carbon is above ground carbon stock per tree in Kg
β_0 is intercept
β_1 is coefficient of CPA
β_2 is coefficient of LiDAR and Aerial derived tree height

Table 13: Regression analysis of four tree species and summary statistics of model using aerial data

Species	β0	β1	β2	R sq	Adj. R sq	Std.error	Obs
Pinus uncinata	-0.544	0.515	1.288	0.49	0.48	0.38	80
Pinus sylvestris	0.398	0.722	1.062	0.46	0.44	0.52	70
Fagus sylvatica	-3.184	0.701	2.288	0.90	0.88	0.26	16
Larix decidua	-1.959	2.371	0.332	0.88	0.85	0.5	10

Table 14: Regression analysis of four tree species and summary statistics of model using LiDAR data

Species	β0	β1	β2	R sq	Adj. R sq	Std.error	Obs
Pinus uncinata	-0.804	0.361	1.545	0.46	0.45	0.39	80
Pinus sylvestris	-0.152	1.789	0.157	0.44	0.42	0.62	70
Fagus sylvatica	-3.479	0.925	2.036	0.89	0.88	0.29	16
Larix decidua	-1.635	2.147	0.395	0.73	0.65	0.69	10

Models for each species and regression coefficient were tested using the F-test and t-test respectively. All the models and regression coefficients were shown to be statistically significant at 95% confidence level.

The developed models were used to predict carbon for the validation dataset, which was plotted against the observed carbon from the field as a way of testing the accuracy of the models. Independent datasets (30%) of the sample data (n=37, *Pinus uncinata*; n=23, *Pinus sylvestris*; n=10, *Fagus sylvatica* and n=5, *Larix decidua*) were used for validating the regression model as described in Table 15.

Table 15: Summary of model validation using aerial image and LiDAR data

Species	**Coefficient of determination**	**Calculated mean carbon**	**RMSE**	**RMSE %**	**Obs.**	**Dataset**
P.uncinata	0.57	31.54	9.61	30.48	37	**Aerial image**
P.sylvestris	0.74	81.45	17.08	20.97	23	
F.sylvatica	0.84	54.49	19.61	35.98	10	
L.decidua	0.88	180.13	97.92	45.95	5	
P.uncinata	0.54	34.82	9.75	28.00	37	**LiDAR**
P.sylvestris	0.57	76.57	29.48	38.50	23	
F.sylvatica	0.71	49.44	16.99	34.38	10	
L. decidua	0.72	185.14	97.47	47.95	5	

Observed and predicted carbon stock from the regression models were plotted against each other as shown in Figure 20 and the coefficient of determination (R^2) was calculated to see the goodness of fit. Root Mean Square Error (RMSE) was used to test for the amount of error in the model. *Larix decidua* and *Fagus sylvatica* showed the best fit of the model in both datasets. Multiple regression models had the lowest RMSE % *i.e*. 20.97% and 30.48% for *Pinus sylvestris* and *Pinus uncinata* respectively. This means that there is 20.97% and 30.48%

average error in the prediction of carbon for *Pinus sylvestris* and *Pinus uncinata* in the case of aerial image. The model error varies from 9.61 to 97.92 kg/tree depending on the species and calculated mean carbon stock in the case of the aerial image data. Similarly, the model error varies from 9.75 to 132.87 kg/tree depending on the species and calculated mean carbon stock in the case of the LiDAR data.

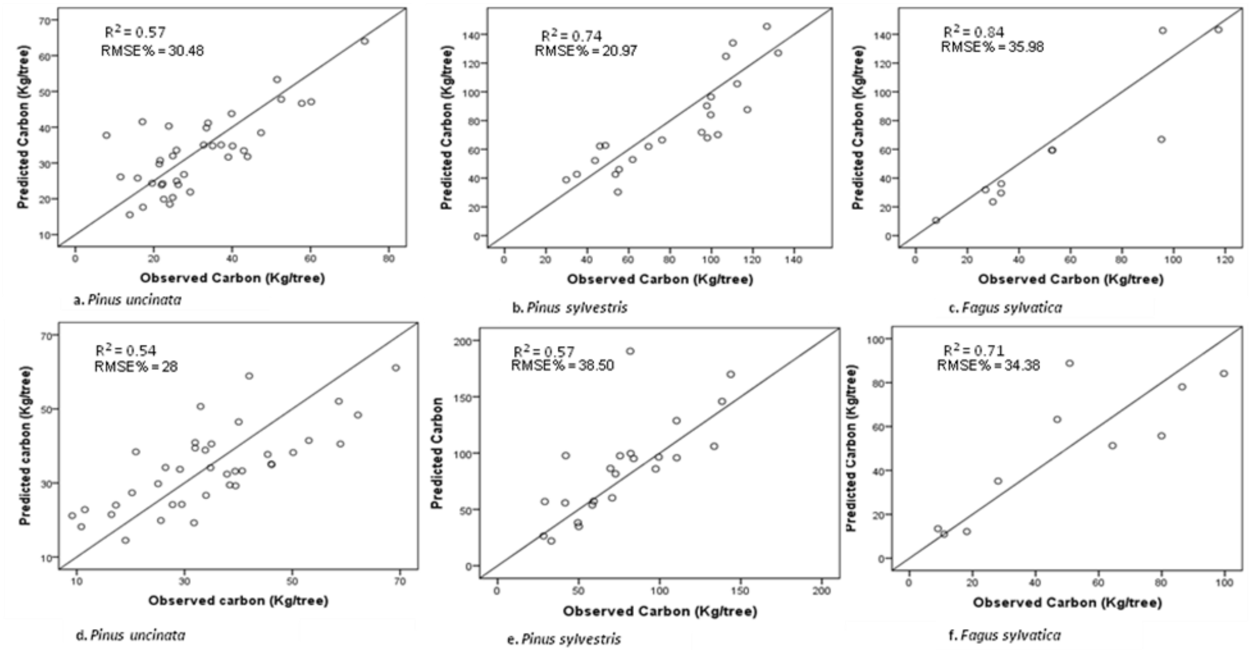

Figure 20: Scatter plot of observed and predicted carbon stock. Top (a, b & c): Aerial Image and Bottom (d, e & f): LiDAR

3.1.9 Carbon stock mapping

The multiple regression models developed for each species were used to estimate total carbon stock in the study area. The total carbon in the study area using aerial image and LiDAR datasets were 7,044,257 kg and 655,025.3 kg respectively. The study area was of 1.3 km^2 (130 ha) thus the study area has approximately 54.18 tonne C ha^{-1} and 47.37 tonne C ha^{-1} respectively using aerial image and LiDAR datasets respectively. Figure 21 shows the carbon stock map of the study area from LiDAR dataset. The carbon stock map of the study area using aerial images is shown in Appendix 7.

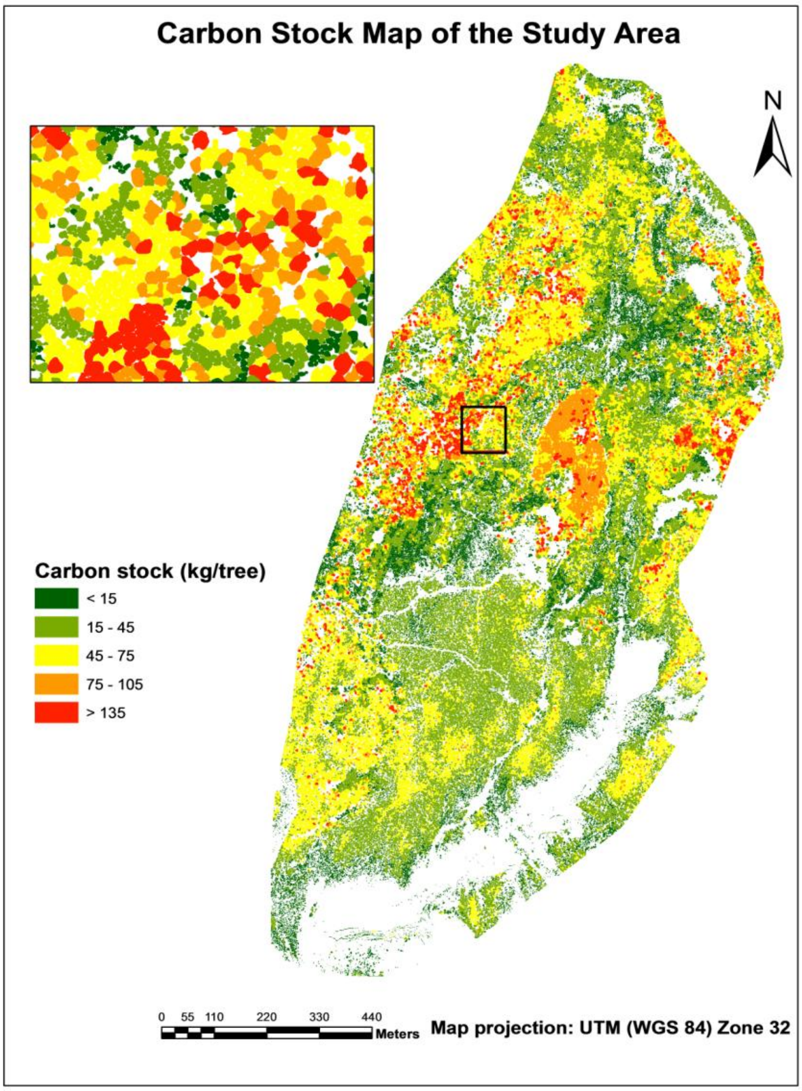

Figure 21: Carbon stock map of the study area

Chapter 4

4.1 DISCUSSION

4.1.1 CHM preparation and accuracy assessment from both datasets

The LiDAR derived canopy height model (CHM) and CHM derived from the photogrammetrically matching of aerial images have been described and reported in this study. The LiDAR derived tree height was underestimated relative to field measured height by 0.10 m on average. Similarly, there was also an underestimation of the photogrammetrically derived tree height by 0.66 m on average. Tree heights extracted from CHM of LiDAR and Aerial Images were evaluated by plotting against field measured height of 340 sampled trees in a scatterplot. Comparision of the LiDAR derived tree height with the field measured tree height resulted in a coefficient of determination (R^2) of 0.81 with RMSE of ±1.18 m. Likewise, regression model assessment between the aerial derived tree height and the field measured tree height showed the coefficient of determination (R^2) 0.66 with RMSE of ±1.69 m. An F-test revealed that there is a statistically significant difference between the tree height derived from LiDAR and the tree height derived from 3D aerial point clouds ($P<0.05$). However, there is no significant difference between the height measured in the field and the height derived from LiDAR ($P<0.05$). There is a significant difference between the height measured in the field and the height derived from 3D aerial point clouds ($P<0.05$). Thus, LiDAR derived tree height was closer to the field measured tree height than the tree height derived from 3D aerial point clouds. Hyyppä et al. (2000) and Persson et al. (2002) also found that the accuracy of the ground measurements is comparable to the height estimations from the LiDAR data. Comparing the correlation between measured and predicted tree heights using LiDAR data, the broadleaved and conifer trees have the value of 0.93 and 0.9 respectively. Similarly, with 3D point clouds of aerial image, the correlation between measured and predicted tree heights of conifers is slightly greater than that of broadleaved trees (0.81 and 0.79 respectively).

Previous studies have shown a high correlation between tree measurements acquired from LiDAR and tree height derived from 3D point cloud of aerial image. Heurich et al. (2004) obtained 0.96 and 0.98 coefficient of determination (R^2) for coniferous and deciduous trees respectively using 10 m point density. They used Vertex III system for the field height measurements and found RMSE of 1.40 m. Erdody and Moskal (2010) found R^2 value of 0.93 from LiDAR derived tree height in coniferous forest using FUSION software and they used an Impulse laser range-finder for measuring tree height. In this study, a high density of LiDAR data with an average of 164 points/m^{-2} was used and showed R^2 of 0.81 which was lower than that of (Heurich et al., 2004) and Erdody and Moskal (2010). We used Haga in this study to measure the tree height in the field and LasTools for processing LiDAR data which could explain the inconsistence with our findings with the abovementioned results. Similarly, Kwak et al. (2007) found R^2 ranging from 0.77 to 0.80 for coniferous species and 0.74 for deciduous species. The accuracy of the tree height estimates in this study is also comparable to the accuracy of the tree height estimations achieved by Razak et al. (2011) with R^2 of 0.72 to 0.91 and RMSE of ±1.07 to ±1.28 m. In this study, the underestimation of LiDAR derived tree heights can be explained by penetration through the canopy and failure to sample treetops caused by the conical shape of conifer trees.

Nurminen et al. (2013) obtained coefficient of determination (R^2) of 0.98 with RMSE of ±1.11 m in the pine forest using 3D point cloud of aerial image having 155 points/m^{-2} point density. Similarly, Dandois and Ellis (2010) obtained an accuracy of field and CHM derived from photogrammetric matching of digital photographs of 0.63 to 0.84 coefficient of determination (R^2) using high sampling density (*i.e.* 30 – 67 points/m^{-2}) in temperate deciduous forest in Maryland USA. The coefficient of determination (R^2) found in this study with 3D point clouds of aerial image is lower than R^2 value obtained by Nurminen et al. (2013). This is because of the low aerial point density we have obtained in this study. The coefficient of determination found in this study is in the range of the values found in the study carried out by Bohlin et al. (2012). However, comparison cannot be done directly because of different forest types, densities, and composition of tree species, topographic features and quality (point density) of LiDAR as well as aerial image.

Density of the point cloud is expected to be one of the main factors for determining the accuracy of tree height (Hyyppä et al., 2008). A higher point density results in a denser point cloud from which a more accurate CHM can be interpolated (Heritage & Large, 2009). In this study, the aerial image has point density of 16.4 points/m^{-2} which was less than the LiDAR point density. When a lower point density is used, the interpolated CHM can result in significant errors (Gaulton & Malthus, 2008). Thus, in this study the underestimation of tree height was greater in case of photogrammetrically derived tree heights than that of LiDAR derived tree heights. The interpolation of poorly matched points result in a low quality of the digital surface model (DSM) from aerial point cloud which later gives a relatively poor CHM. Yu et al. (2004) found the underestimation of height increased with higher flying heights because of lower sampling density. In addition, Lefsky et al. (2002) and Persson et al. (2002) also pointed the underestimation of height due to low sampling density. The point cloud resulted from photogrammetric matching of aerial images only has single return which might have impact on accuracy of DTM generation while LiDAR data has multiple returns, which makes it possible to generate the

DTM more accurately (Lisein et al. 2013). Additional error in the underestimation of heights from both datasets could be due to the gap (2 to 4 years) between when these two datasets were co-captured in July 2009 and when field data were collected in 2012 and 2013. LidAR point cloud is a direct measurement while 3D photogrammetry matching point cloud is a derived estimation.

Different types of error can be attributed to tree height measurements. The dominant source of error in LiDAR and aerial tree height measurement is due to the difficulty in measuring treetop location and error in the DTM at the base of the tree. The errors in the LiDAR derived measurement due to ground vegetation and terrain micro-relief can introduce up to 0.5 m of variability in height measurements (Leckie et al., 2003). However, with high sampling density the errors in terrain models are unlikely to produce errors greater than 0.30 m (Reutebuch et al., 2003). Apart from that, it is often challenging in the field to identify the highest point of the tree crown because of no distinct peak. This was observed in the field when trees are leaning or have large crowns with irregular shape (Figure 22). In addition, the interlocking of branches of different trees also makes it difficult to extract single tree heights (Hollaus et al., 2007).

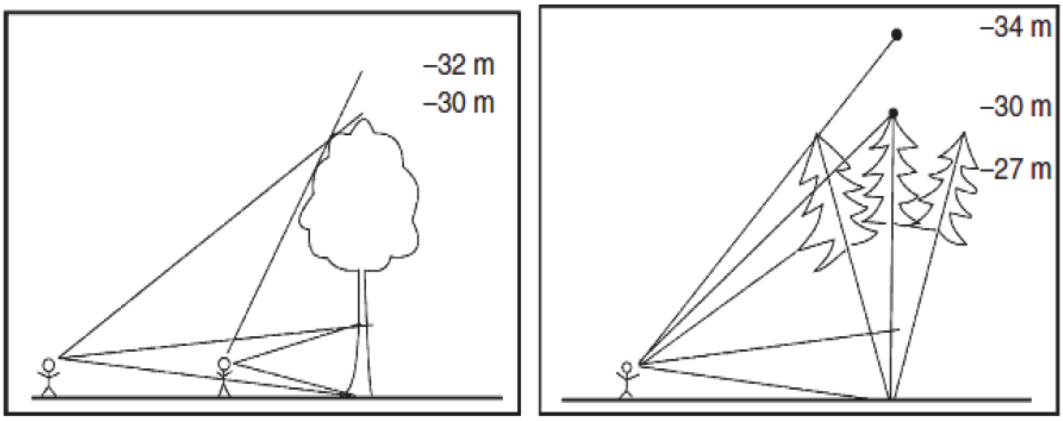

Figure 22: Errors in tree height measurements (Köhl et al., 2006)

Tree height is an important variable in forest inventory programs. There are several instruments that are commonly used for measuring height in field, for example handheld instruments such as the Suunto hypsometer and Haga hypsometer. More precise, expensive and stable instruments such as the theodolite or total station can be used, but for routine work, this is impractical because of the expense and time required to make measurements of individual trees. Previous studies (Hyyppä et al., 2000; Maltamo et al., 2004) have shown a high correlation between tree measurements acquired from LiDAR and those acquired in field using handheld instruments. However, which of the two is the true height is questionable. In this study, Haga hypsometer was used to estimate tree height in the field. Hunt (1959) reported that the Haga altimeter measure the tree height more precisely than most other handheld instruments.

To investigate whether field measurement with a handheld instrument or the LiDAR derived height is the true height, a small experiment was conducted with measurements of some trees and buildings in the neighbourhood of the ITC building (Appendix 8). The heights of eight trees and two buildings were estimated with a Haga hypsometer and also measured with a Wild T05 theodolite. Although it is not a precision theodolite (which can measure horizontal and vertical angles with a precision of ± one second of arc), the instrument can measure with a precision of ± 2 minutes of arc. At a typical horizontal distance of 50 m, a vertical angle of 2 minutes of arc means that heights can be measured to within 50 m × tan 2′ = ±0.03m.

The LiDAR data for this experiment was the *Actueel Hoogtebestand Nederland* (AHN). This has a specified accuracy of ± 0.05 m standard deviation and ± 0.05 m systematic error (Swart, 2010). The CHM was prepared for a small area covering van Heek Park and the ITC building with 9.9 points m^{-2}. Coefficient of determination (R^2) between T05 theodolite and LiDAR derived height was 0.97 and RMSE of ±1.12 was obtained. The LiDAR derived height was underestimated by 0.43 m on average. Similarly, Coefficient of determination (R^2) between T05 theodolite and Haga derived height was 0.97 and RMSE of ±1.19 was obtained. On average mean value of Haga derived height was 0.57 m greater than the theodolite height. Summary of statistics for tree height measurements presented in Appendix 9.

This small experiment suggests that the LiDAR derived height is closer to the field height measured by theodolite than the field height measured by handheld Haga. The significant portion of the RMSE could be caused by uncertainty in the field height measurements for example in identifying the exact top of the tree. In our present study, we found there is no significant difference in mean heights between LiDAR derived tree height and field measured tree height.

4.1.2 Image segmentation and accuracy assessment

Several methods exist for detecting and segmenting trees on the image. In this study, region growing approach was used for the tree crown delineation of LiDAR and aerial image, which is explained in section 2.1.3.7 and results are presented in section 3.1.6. Erikson (2003) showed the superiority of the Region Growing method over other approaches. Region growing works well with correct delineation as much as 95% of all visible tree crown segmentation of images (Erikson, 2003).

Several criteria have been used for quantitative evaluation of segmentation accuracy as represented by Möller et al. (2007) and Clinton et al. (2010). In this study, we adopted the methods presented by Zhan et al. (2005) *i.e* 1:1

spatial correspondence and Clinton et al. (2010) measure of closeness index *i.e.* goodness of fit between manually delineated polygons and segmented polygons for accuracy assessment of segmentation. Measure of closeness index with LiDAR data showed 67% accuracy with 0.33 D value whereas aerial image showed 70% accuracy with 0.30 D value. Likewise, 1:1 spatial correspondence showed 77% and 80% accuracy for LiDAR and aerial image respectively.

The finding of this study can be compared with different studies carried out by several researchers (Maharjan, 2012; Wang et al., 2004; Workie, 2011). Wang et al. (2004) in their study obtained 75% segmentation accuracy for the spruce and fir forests of British Columbia, Canada. Similarly, Maharjan (2012) achieved segmentation accuracy of 76% by applying 1:1 correspondence method using region growing approach in the hilly forest of Gorkha, Nepal. Workie (2011) in his study achieved 80% segmentation accuracy in terms of 'goodness of fit' for coniferous trees using combined valley following and marker free watershed transformation. Ke and Quackenbush (2008) obtained relatively low segmentation accuracy of 61% in mixed forest of broadleaf and conifer. The segmentation accuracy of this study is with agreement with the result obtained by Hatami (2012) in the same study. She found the segmentation accuracy of 79% in terms of 1:1 correspondence. Higher accuracy was expected because of high point density. The segmentation accuracy is found to be higher in aerial image than LiDAR. This may partly be a consequence of delineating the ground reference properly in the case of aerial image because of multispectral and spatial detail. The aerial image produced a better isolation in the more dense stands (Leckie et al., 2003). However, the use of height information helped to separate trees from other ground vegetation. Thus, the height from LiDAR data is combined with image to eliminate commission errors that often occur in open stand with optical imagery (Leckie et al., 2003).

In this study, the segmentation result showed over-segmentation and under-segmentation errors. The under-segmentation errors were higher in this study from both datasets because of inability to separate neighbouring trees. For the small tree crowns, the ground reference data and corresponding automated segmentation matched properly but for large crowns, individual large branches can cause the algorithms to split trees into several entities. This will lead to over-segmentation errors (Figure 23a). This makes it difficult to parameterize the algorithm to produce good results where there is a mixture of crown sizes and irregular shape of crown. Similarly, under-segmentation errors were also observed (Figure 23b) when the algorithm, instead of splitting the neighbouring trees, made one segment for two trees and in some part, more than two. Thus, the segmentation accuracy can be misleading because of the accommodated over-segmentation and under-segmentation errors. The forest density also influenced the performance of algorithms. Trees stand which are close to each other have their tree crowns intermingled which made it difficult to visually separate tree clusters into individual trees (Ke & Quackenbush, 2008).

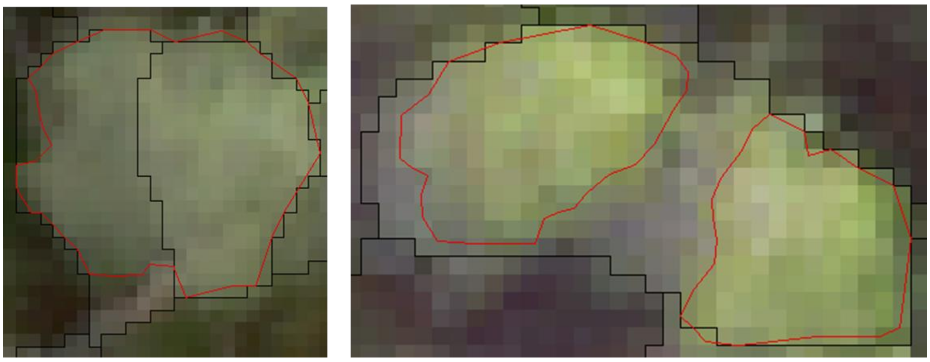

a. Commission error b. Omission error
(Red polygons represent manually delineated crown and black polygon represent automated segments)
Figure 23: Example of commission and omission error

Apart from this view angle causes difficulties with tree crown delineation on both the LiDAR and aerial imagery. Different parts of the crown as well as crown outlines are visible depending on view angle and it makes a tree look different when it at nadir or at sunlit side (Leckie et al., 2003). In addition to this, distortion present in imagery (Figure 24) in some parts of the study area also hinder the algorithm in eCognition so that the tree crown were not segmented properly and it misled the segmentation accuracy.

Figure 24: Image distortion

4.1.3 Model development and validation

The relationships among the variables DBH, CPA, AGB, and CHM of both the aerial image and LiDAR datasets were evaluated using correlation analysis (Table 11 & 12). This correlation analysis demonstrated that in almost all cases, the strength of the linear relationship between DBH and carbon (>0.70) is highly significant ($P<0.01$) for all four species in the aerial and LiDAR datasets. However, the correlation value of 0.63 was obtained in the case of *Fagus sylvatica* using LiDAR data. It was as expected that as DBH is one of the strong predictors to measure above ground biomass (Rutishauser et al., 2013). Therefore, there is no significant difference in correlation values among these variables in both datasets. The correlation coefficient of CPA with carbon and CPA with height was found to be less than that of DBH with carbon for both datasets. The correlation coefficient between CPA and carbon is more than 0.60 in particular for the *Fagus sylvatica* and *Larix decidua* in both aerial and LiDAR datasets. Coefficient of determination (R^2) was found low in this study between CPA and carbon while Kuuluvainen (1991) obtained R^2 of 0.79 for a Norway spruce plantation using the model of CPA and AGB. Coefficient of determination (R^2) obtained for the relationship between height and carbon was 0.41, 0.41, 0.79 and 0.69 for *Pinus uncinata*, *Pinus sylvestris*, *Fagus sylvatica* and *Larix decidua* respectively which is comparable to the R^2 obtained by Yu et al. (2010) who obtained R^2 of 0.6 in the mixed forest in the north-eastern United states.

Multiple regression models were applied to know the combined effect of both the predictor variables in order to estimate carbon stock which ensures better prediction (Ketterings et al., 2001). Both CPA and height derived from both LiDAR and aerial image were used to predict the carbon stock of four different tree species present in the study area. A log transformed multiplicative model was preferred to predict the carbon stock to reduce bias in estimating biomass of tree as indicated by previous studies (Feldpausch et al., 2012; Means, 2000). A log transformation is recommended to correct the skewness of data which do not fit with the requirements for parametric statistical tests (Keene, 1995). Watt and Kirschbaum (2011) obtained R^2 value of 0.73 between height and DBH of even aged coniferous stands after performing log transformation to both the variables.

Coefficients of determination (R^2) for the model using aerial image were 0.57, 0.74, 0.84 and 0.88 for *Pinus uncinata*, *Pinus sylvestris*, *Fagus sylvatica* and *Larix decidua* respectively. This means 57%, 74%, 84% and 88% of the variation in carbon can be explained by CPA and height for *Pinus uncinata*, *Pinus sylvestris*, *Fagus sylvatica* and *Larix decidua* respectively. Similarly, in the case of the LiDAR data, 54%, 57%, 71% and 72% of the variation in carbon can be explained by CPA and height for *Pinus uncinata*, *Pinus sylvestris*, *Fagus sylvatica* and *Larix decidua* respectively. This result is similar to the result found by Hatami (2012) in the same study area where she found R^2 of

0.56 for pine species. The overall R^2 value was 0.76 and 0.65 for aerial image and LiDAR datasets which can be compared to that of the results (0.75) obtained by Kumar (2012) in the same study area. In this study, the allometric equation for *Pinus sylvestris, Fagus sylvatica* and *Larix decidua* were taken from Italy, and allometric equation for *Pinus uncinata* was taken from Spain while Kumar (2012) used allometric equation of *Pinus nigra* for *Pinus uncinata* from Netherlands and he used different model based on height, CPA and local tree density. The result from this study is compared with the study done by Kuuluvainen (1991) who found R^2 ranging from 0.22 to 0.79 in a Norway spruce in Switzerland. Results of this study are relatively lower in comparison to Zhao et al. (2009) who found R^2 value ranging from 0.80 to 0.95 for pine trees when modelling carbon stock using LiDAR derived heights.

The coefficient of determination (R^2) and RMSE show how accurately carbon stock of the forest can be predicted from the regression model. The lowest RMSE % *i.e*. 20.97% and 30.48% was obtained for *Pinus sylvestris* and *Pinus uncinata* respectively using the aerial image. This shows that there were 20.97% and 30.48% average error in the prediction of carbon for *Pinus sylvatica* and *Pinus uncinata* in the case of aerial data. Similarly, the result showed 38.5% and 28% average error in the prediction of carbon for *Pinus sylvatica* and *Pinus uncinata* in the case of the LiDAR data. Validation of the models resulted in the highest value of RMSE for *Larix decidua* (97.92 kg/tree and 97.47 kg/tree) using aerial and LiDAR datasets respectively. The highest error can be attributed to the small sample size (5) used for the validation. In terms of the aerial image, it indicated that on average carbon stock can be predicted with 75% variability and 35% RMSE from the model developed for each species. Similarly, in terms of LiDAR data, it indicated that on average carbon stock can be predicted with 64% variability and 39% RMSE from the model developed for each species. Thus, height and CPA will give a good estimate of biomass and can better explain about variability of biomass than the use of CPA or tree height alone.

4.1.4 Carbon stock estimation

In this study, approximately 54.18 tonne C ha^{-1} of carbon stock was estimated using segmented CPA and height derived from aerial point clouds. Similarly, approximately 47.37 tonne C ha^{-1} of carbon stock was estimated using segmented CPA and height derived from LiDAR. The estimated carbon stock in this study is in agreement with the estimated carbon stock obtained by Hatami (2012). She obtained approximately 52.88 tonne C ha^{-1} using the same model in the same study area. The result obtained in this study can also be compared with the result obtained by Kumar (2012) where he used a different model and different allometric equations. He got the estimated carbon stock of 29.32 tonne C ha^{-1} which is lower than our study. Our result is also within the ranges of mean carbon stock per hectare calculated for French forest (48.3 tonne C ha^{-1} to 59 tonne C ha^{-1}) (Pignard et al., 2000). The differences in biomass estimation in this study are because it attributed to the four different tree species in the study area while Kumar (2012) estimated carbon stock for Pine trees only. The mean carbon/tree for *Pinus uncinata* and *Pinus sylvestris* is 31.54 kg and 81.45 kg respectively in the case of the aerial image and 34.82 kg and 76.57 kg respectively in the case of the LiDAR which is comparable to 55.6 and 65.5kg for *Pinus uncinata* and *Pinus sylvestris* respectively (Hatami, 2012). Kim et al. (2010) obtained 193 kg for *Pinus densiflora* with mean DBH of 40 cm and mean height 17.2 m. The difference in carbon stock in the study area of these two datasets is mainly due to the segmentation of the shadow area in the aerial image which would affect the total number of trees in the study area and eventually the carbon stocks.

4.1.5 Sources of error or uncertainties

There are several uncertainties associated with the estimation of above ground carbon in the forest. The sources of error may ranges from the data collection in the field to data acquisition, image processing and model development for carbon estimation. Some of the errors which introduced at several steps of research are highlighted in the following subsections.

GPS error

The orthophoto and coordinate of each sample plot was used to navigate the sample tree location in the forest using GPS. The GPS signal can, however, be disturbed by various factors such as topographic features, density of forest, atmospheric conditions, satellite position, noise in the radio signal and natural barriers to the signal (Karna, 2012). Noise can create an error between 1 to 10 meters and barriers between satellite and receiver can produce error up to 30 m. The errors are more profound in mountainous area which can produce error up to 30 m (maps-gps-info.com, 2014). Some degrees of uncertainties were also prevalent as the GPS signal was degraded by forest canopies and clouds particularly in plots where there were overlapping crowns.

Allometric equation for carbon estimation

Forest tree biomass estimates depend upon allometric equations that are developed from a limited region or a broader combination of sites using a finite number of individuals (Chambers et al., 2001). However, those allometric equations are often applied beyond the regions for which they were developed as well as beyond the range of diameters sampled (Chave et al., 2004). Unfortunately, allometric equations were not available for this study area. Therefore, allometric equations from Italy and Spain were taken for the estimation of biomass. Though the region from where these allometric equations are developed share the same climate, those allometries are based on significantly larger sample size. So the allometric equation developed for one area may produce extrapolation errors when applied beyond the range of region and model development data (Andersen et al., 2005). Thus, one of the sources in biomass estimation can be attributed to allometric equation.

Uncertainty on tree level estimation

The accuracy of biomass estimation for individual trees depends on the accuracy of tree height measurements. Tree height and DBH are the most commonly used variables to predict AGB but height measurements are dependent on forest conditions, observer experience and the equipment used which introduces the error at initial stage. Thus, error propagates from measurement in the field. Likewise, due to the deformity of trunk at breast height or irregularity in trunk shape, the measurement of DBH of trees could be wrong. Thus, this possess systematic errors and can affect the quality of regression model and ultimately the overall estimation of carbon stock for individual tree (Zhang et al., 2010).

Other errors/ uncertainty

Noise on LiDAR data and Aerial image is also a limitation which cannot allow accurate biomass estimation. Though, the filter was applied, still some pixels with wrong values remain. The CHM derivation from LiDAR point cloud and aerial point cloud accumulate some errors while extracting based on each centre point of polygon and those errors can propagate in the further step (Nguyet, 2012). Accurate tree crown delineation is a key factor for estimating biomass based on CPAs derived from image segmentation (Ke & Quackenbush, 2008). Over-segmentation and under-segmentation were observed due to overlapping trees and branches of big trees which can grow into irregular shape and thus affect the relationship between AGB and CPA.

Chapter 5

5.1 CONCLUSION AND RECOMMENDATIONS

5.1.1 Conclusion

This research has emphasized the potentials of high density point cloud LiDAR data and photogrammetric matching of aerial images for estimating above ground carbon stock of Bois noir forest of Barcelonnette. This study clearly shows the potential of these two datasets to extract the forest attributes: height and CPA. However, the biomass estimation with these two datasets could not explain which one is more accurate but the substantial economic and logical costs incurred by LiDAR data can be overcome by inexpensive aerial 3D measurements.

The result showed that LiDAR derived tree height was able to explain 81% of field measured tree height with RMSE of 1.18 m. While, tree height derived from 3D aerial point clouds was able to explain 66% of field measured tree height with RMSE of 1.69 m. Pearson's correlation analysis indicated statistically significant correlation between field tree height and LiDAR derived tree height at $P<0.05$ whereas t-test showed no difference between means of field measured tree heights and tree heights derived from LiDAR point clouds.

Two types of accuracy assessment for segmentation of the image were applied in this study i.e. measure of closeness (D value) and 1:1 spatial correspondence. Overall D value for the study area using LiDAR data was found to be 0.33 with 0.31 over segmentation and 0.35 under segmentation that means there was 33% error (67% accuracy) in segmentation whereas 77% accuracy of segmentation was obtained from 1:1 spatial correspondence. However, overall D value for the study area using aerial image was found to be 0.30 with 0.28 over segmentation and 0.33 under segmentation that means there was 30% error (70% accuracy) in segmentation whereas 80% accuracy of segmentation was obtained from 1:1 spatial correspondence. There was no significant difference between LiDAR and aerial photos in segmenting tree crowns at 95% confidence level.

Pearson's correlation analysis indicated that there is a strong positive correlation ($r>0.90$) between field measured diameter and carbon for almost all of the tree species in both datasets. The result also showed that the correlation between height derived from 3D aerial point cloud and LiDAR with carbon was higher than the correlation between automated segmentation of crown projection area and carbon.

Model validation results showed that species wise regression model were able to explain up to 57%, 74%, 84% and 88% of variation in carbon estimation for *Pinus uncinata, Pinus sylvestris, Fagus sylvatica* and *Larix decidua* respectively in the case of aerial image. Similarly, 54%, 57%, 71% and 72% of variation in carbon estimation for *Pinus uncinata, Pinus sylvestris, Fagus sylvatica* and *Larix decidua* respectively was explained by the model in the case of LiDAR data. There was no significant difference in carbon estimation between two datasets. The regression model developed is used to estimate the AGB carbon of each individual tree in the study area. The total amount of carbon stock in the study area with aerial image and LiDAR was 54.18 tonne C ha^{-1} and 47.37 tonne C ha^{-1} respectively.

5.1.2 Recommendations

1. 3D photogrammetric matching of aerial image offers a potential approach for modelling forest AGB / carbon stock like LiDAR. It can replace the cost incurred by LiDAR in data acquisition. Further study should be done to check its accuracy for extracting essential forest related information in terms of time and cost.

2. The allometric equation used in this study was not site specific which will bring errors in the developed models. Therefore, there is a need to develop site specific and species specific allometric equations for accurate carbon estimation.

3. Differential GPS (DGPS) should be used for an accurate field validation which could minimize the field based location error and recognition of the individual trees on image.

4. Further investigation on the effect of variable window sizes in the local maximum filtering strategy should be done to locate treetops on both the LiDAR CHM and the orthophoto.

References

Ackermann, F. (1999). Airborne laser scanning - present status and future expectations. *ISPRS Journal of Photogrammetry and Remote Sensing, 54*(2-3), 64-67. doi: 10.1016/s0924-2716(99)00009-x

Aldred, A. H. (1978). *Application of large-scale photos to a forest inventory in Alberta / by A. H. Aldred and J. J. Lowe*. Ottawa: Canadian Forestry Service, Environment Canada.

Andersen, H.-E., McGaughey, R. J., & Reutebuch, S. E. (2005). Estimating forest canopy fuel parameters using LIDAR data. *Remote Sensing of Environment, 94*(4), 441-449.

Avery, T. E. (1969). *Forester's guide to aerial photo interpretation*. Washington, D.C.: U.S. Dept. of Agriculture, Forest Service.

Baccini, A., Friedl, M. A., Woodcock, C. E., & Warbington, R. (2004). Forest biomass estimation over regional scales using multisource data. *Geophysical Research Letters, 31*(10). doi: 10.1029/2004gl019782

Baltsavias, E. P. (1999). A comparison between photogrammetry and laser scanning. *ISPRS Journal of Photogrammetry and Remote Sensing, 54*, 83-94. doi: 0924-2716/99

Balzter, H., Rowland, C. S., & Saich, P. (2007). Forest canopy height and carbon estimation at Monks Wood National Nature Reserve, UK, using dual-wavelength SAR interferometry. *Remote Sensing of Environment, 108*(3), 224-239. doi: 10.1016/j.rse.2006.11.014

Bohlin, J., Wallerman, J., & Fransson, J. E. S. (2012). Forest variable estimation using photogrammetric matching of digital aerial images in combination with a high-resolution DEM. *Scandinavian Journal of Forest Research, 27*(7), 692-699. doi: 10.1080/02827581.2012.686625

Bonnor, G. M. (1985). *Inventory of forest biomass in Canada*: Canadian Forestry Service.

Brandtberg, T., Warner, T. A., Landenberger, R. E., & McGraw, J. B. (2003). Detection and analysis of individual leaf-off tree crowns in small footprint, high sampling density lidar data from the eastern deciduous forest in North America. *Remote Sensing of Environment, 85*(3), 290-303.

Brown, S., & Gaston, G. (1996). Estimates of biomass density for tropical forests. *Biomass burning and global change, 1*, 133-139.

Brown, S., Gillespie, A. J., & Lugo, A. E. (1989). Biomass estimation methods for tropical forests with applications to forest inventory data. *Forest science, 35*(4), 881-902.

Chambers, J. Q., Santos, J. d., Ribeiro, R. J., & Higuchi, N. (2001). Tree damage, allometric relationships, and above-ground net primary production in central Amazon forest. *Forest Ecology and Management, 152*(1), 73-84.

Chave, J., Condit, R., Aguilar, S., Hernandez, A., Lao, S., & Perez, R. (2004). Error propagation and scaling for tropical forest biomass estimates. *Philosophical Transactions of the Royal Society of London. Series B: Biological Sciences, 359*(1443), 409-420.

Chen, Q., Baldocchi, D., Gong, P., & Kelly, M. (2006). Isolating individual trees in a savanna woodland using small footprint lidar data. *Photogrammetric Engineering and Remote Sensing, 72*(8), 923-932.

Chen, Q., Vaglio Laurin, G., Battles, J. J., & Saah, D. (2012). Integration of airborne lidar and vegetation types derived from aerial photography for mapping aboveground live biomass. *Remote Sensing of Environment, 121*(0), 108-117. doi: http://dx.doi.org/10.1016/j.rse.2012.01.021

Clinton, N., Holt, A., Scarborough, J., Yan, L., & Gong, P. (2010). Accuracy assessment measures for object-based image segmentation goodness. *Photogrammetric Engineering and Remote Sensing, 76*(3), 289-299.

Culvenor, D. S. (2002). TIDA: an algorithm for the delineation of tree crowns in high spatial resolution remotely sensed imagery. *Computers & Geosciences, 28*(1), 33-44. doi: 10.1016/s0098-3004(00)00110-2

Dandois, J. P., & Ellis, E. C. (2013). High spatial resolution three-dimensional mapping of vegetation spectral dynamics using computer vision. *Remote Sensing of Environment, 136*(0), 259-276. doi: http://dx.doi.org/10.1016/j.rse.2013.04.005

Definiens. (2007). *Definiens Developer 7: Reference Book*. Munich, Germany.

Dong, J. R., Kaufmann, R. K., Myneni, R. B., Tucker, C. J., Kauppi, P. E., Liski, J., Buermann, W., Alexeyev, V., & Hughes, M. K. (2003). Remote sensing estimates of boreal and temperate forest woody biomass: carbon pools, sources, and sinks. *Remote Sensing of Environment, 84*(3), 393-410. doi: 10.1016/s0034-4257(02)00130-x

Drake, J. B., Dubayah, R. O., Knox, R. G., Clark, D. B., & Blair, J. (2002). Sensitivity of large-footprint lidar to canopy structure and biomass in a neotropical rainforest. *Remote Sensing of Environment, 81*(2), 378-392.

eCognition. (2011). *eCognition Developer 8.7: User Guide*. Munich, Germany.

Erdody, T. L., & Moskal, L. M. (2010). Fusion of LiDAR and imagery for estimating forest canopy fuels. *Remote Sensing of Environment, 114*(4), 725-737.

Erikson, M. (2003). Segmentation of individual tree crowns in colour aerial photographs using region growing supported by fuzzy rules. *Canadian Journal of Forest Research, 33*(8), 1557-1563.

Evans, J. S., Hudak, A. T., Faux, R., & Smith, A. (2009). Discrete return LiDAR in natural resources: recommendations for project planning, data processing, and deliverables. *Remote Sensing, 1*(4), 776-794.

Fauvart, N., Ali, A. A., Terral, J. F., Roiron, P., Blarquez, O., & Carcaillet, C. (2012). Holocene upper tree-limits of Pinus section sylvestris in the Western Alps as evidenced from travertine archives. *Review of Palaeobotany and Palynology, 169*, 96-102. doi: 10.1016/j.revpalbo.2011.10.003

Feldpausch, T. R., Lloyd, J., Lewis, S. L., Brienen, R., Gloor, E., Mendoza, A. M., Lopez-Gonzalez, G., Banin, L., Salim, K. A., & Affum-Baffoe, K. (2012). Tree height integrated into pan-tropical forest biomass estimates. *Biogeosciences Discussions, 9*(3).

Flageollet, J. C., Maquaire, O., Martin, B., & Weber, D. (1999). Landslides and climatic conditions in the Barcelonnette and Vars basins (Southern French Alps, France). *Geomorphology, 30*(1-2), 65-78. doi: 10.1016/S0169-555X(99)00045-8

Florinsky, I. V. (1998). Combined analysis of digital terrain models and remotely sensed data in landscape investigations. *Progress in Physical Geography, 22*(1), 33-60. doi: 10.1177/030913339802200102

Gaulton, R., & Malthus, T. J. (2008). *LiDAR mapping of canopy gaps in continuous cover forests: A comparison of canopy height model and point cloud based techniques*.

Gibbs, H. K., Brown, S., Niles, J. O., & Foley, J. A. (Writers). (2007). Monitoring and estimating tropical forest carbon stocks: making REDD a reality. In IOPscience (Producer).

Gini, R., Passoni, D., Pinto, L., & Sona, G. (2012). Aerial images from an UAV system: 3d modeling and tree species classification in a park area. *Int Arch Photogramm Remote Sens Spatial Inf Sci, 39*, B1.

GlobeAllomeTree. (2013). Assessing volume, biomass and carbon stocks of trees and forests. Retrieved on 12 December 2013, 2013, from http://www.globallometree.org/data/search/

Gong, P., Sheng, Y., & Biging, G. S. (2002). 3D model-based tree measurement from high-resolution aerial imagery. *Photogrammetric Engineering and Remote Sensing, 68*(11), 1203-1212.

Gougeon, F. A., & Leckie, D. G. (2006). The individual tree crown approach applied to Ikonos images of a coniferous plantation area. *Photogrammetric Engineering and Remote Sensing, 72*(11), 1287-1297.

Haala, N. (2009). *Comeback of digital image matching.* Paper presented at the Photogrammetric Week.

Haala, N., Hastedt, H., Wolf, K., Ressl, C., & Baltrusch, S. (2010). Digital photogrammetric camera evaluation generation of digital elevation models. *Photogrammetrie-Fernerkundung-Geoinformation, 2010*(2), 99-115.

Hatami, F. (2012). *Carbon estimation of individual trees using high laser density data of airborne LIDAR : a case study in Bois Noir, France.* University of Twente Faculty of Geo-Information and Earth Observation (ITC), Enschede. Retrieved from http://www.itc.nl/library/papers_2012/msc/nrm/hatami.pdf

Heinzel, J. N., Weinacker, H., & Koch, B. (2008). Full automatic detection of tree species based on delineated single tree crowns–a data fusion approach for airborne laser scanning data and aerial photographs. *Proceedings of SilviLaser, 2008*, 8th.

Heritage, G., & Large, A. (2009). *Laser scanning for the environmental sciences*: John Wiley & Sons.

Herwitz, S., Johnson, L., Dunagan, S., Higgins, R., Sullivan, D., Zheng, J., Lobitz, B., Leung, J., Gallmeyer, B., & Aoyagi, M. (2004). Imaging from an unmanned aerial vehicle: agricultural surveillance and decision support. *Computers and Electronics in Agriculture, 44*(1), 49-61.

Heurich, M., Persson, Å., Holmgren, J., & Kennel, E. (2004). Detecting and measuring individual trees with laser scanning in mixed mountain forest of central Europe using an algorithm developed for Swedish boreal forest conditions. *International Archives of Photogrammetry, Remote Sensing and Spatial Information Sciences, 36*, 307-312.

Hollaus, M., Wanger, W., Nmaier, B., & Schadauer, K. (2007). Airborne laser scanning of forest stem volume in a mountainous environment. *Sensors, 7*(8), 1559-1577. doi: 10.3390/s7081559

Houghton, J. T. (1997). *Revised 1996 IPCC guidelines for national greenhouse gas inventories*: Intergovernmental Panel on Climate Change.

Huang, H., Gong, P., Cheng, X., Clinton, N., & Li, Z. (2009). Improving measurement of forest structural parameters by co-registering of high resolution aerial imagery and low density LiDAR data. *Sensors, 9*(3), 1541-1558.

Hudak, A. T., & Wessman, C. A. (2001). Textural analysis of high resolution imagery to quantify bush encroachment in Madikwe Game Reserve, South Africa, 1955-1996. *International Journal of Remote Sensing, 22*(14), 2731-2740. doi: 10.1080/01431160119030

Hunt, E. V. (1959). A time and accuracy test of some hypsometers. *Journal of Forestry, 57*(9), 641-643.

Husch, B., Beers, T. W., & Kershaw, J. A. (2003). *Forest mensuration* (Fourth edition ed.). Hoboken: Wiley & Sons.

Hyde, P., Nelson, R., Kimes, D., & Levine, E. (2007). Exploring LiDAR–RaDAR synergy—Predicting aboveground biomass in a southwestern ponderosa pine forest using LiDAR, SAR and InSAR. *Remote Sensing of Environment, 106*(1), 28-38.

Hyyppä, J., Hyyppa, H., Leckie, D., Gougeon, F., Yu, X., & Maltamo, M. (2008). Review of methods of small-footprint airborne laser scanning for extracting forest inventory data in boreal forests. *International Journal of Remote Sensing, 29*(5), 1339-1366. doi: 10.1080/01431160701736489

Hyyppä, J., Pyysalo, U., Hyyppä, H., & Samberg, A. (2000). *Elevation accuracy of laser scanning-derived digital terrain and target models in forest environment.* Paper presented at the 4th Workshop on lidar remote sensing of land and sea. Dresden, Germany: EARSeL.

IPCC. (2006). 2006 IPCC Guidelines for National Greenhouse Gas Inventories Volume 4 Agriculture, Forestry and other Land Use Retrieved 03 January, 2014,fromhttp://www.ipccnggip.iges.or.jp/public/2006gl/pdf/4_Volume4/V4_04_Ch4_Forest_Land.pdf

IPCC. (2007). Summary for Policymakers. In: Climate Change 2007: The Physical Science Basis. Contribution of Working Group I to the Fourth Assessment Report of the Intergovernmental Panel on Climate Change. Cambridge University Press, Cambridge, United Kingdom and New York, NY, USA.

Järnstedt, J., Pekkarinen, A., Tuominen, S., Ginzler, C., Holopainen, M., & Viitala, R. (2012). Forest variable estimation using a high-resolution digital surface model. *ISPRS Journal of Photogrammetry and Remote Sensing, 74*(0), 78-84. doi: http://dx.doi.org/10.1016/j.isprsjprs.2012.08.006

Jenkins, J. C., Chojnacky, D. C., Heath, L. S., & Birdsey, R. A. (2003). National-scale biomass estimators for United States tree species. *Forest science, 49*(1), 12-35.

Jensen, J. R. (1996). *Introductory digital image processing: a remote sensing perspective*: Prentice-Hall Inc.

Karna, Y. K. (2012). *Mapping above ground carbon using worldview satellite image and LIDAR data in relationship with tree diversity of forests.* University of Twente Faculty of Geo-Information and Earth Observation (ITC), Enschede. Retrieved from http://www.itc.nl/library/papers_2012/msc/nrm/karna.pdf

Ke, Y., & Quackenbush, L. J. (2008). *Comparison of individual tree crown detection and delineation methods.* Paper presented at the Proceedings of 2008 ASPRS annual conference.

Ke, Y., Quackenbush, L. J., & Im, J. (2010). Synergistic use of QuickBird multispectral imagery and LIDAR data for object-based forest species classification. *Remote Sensing of Environment, 114*(6), 1141-1154.

Keene, O. N. (1995). The log transformation is special. *Statistics in medicine, 14*(8), 811-819.

Ketterings, Q. M., Coe, R., van Noordwijk, M., Ambagau, Y., & Palm, C. A. (2001). Reducing uncertainty in the use of allometric biomass equations for predicting above-ground tree biomass in mixed secondary forests. *Forest Ecology and Management, 146*(1), 199-209.

Kim, S. R., Kwak, D. A., oLee, W. K., Son, Y., Bae, S. W., Kim, C., & Yoo, S. (2010). Estimation of carbon storage based on individual tree detection in Pinus densiflora stands using a fusion of aerial photography and LiDAR data. *Science China-Life Sciences, 53*(7), 885-897. doi: 10.1007/s11427-010-4017-1

Kirschbaum, M. (1996). The carbon sequestration potential of tree plantations in Australia. *Environmental Management: the Role of Eucalypts and Other Fast Growing Species, CSIRO Forestry and Forest Products, Canberra*, 77-89.

Köhl, M., Baldauf, T., Plugge, D., & Krug, J. (2009). Reduced emissions from deforestation and forest degradation (REDD): A climate change mitigation strategy on a critical track. *Carbon Balance and Management, 4*. doi: 10.1186/1750-0680-4-10

Köhl, M., Magnussen, S., & Marchetti, M. (2006). *Sampling methods, remote sensing and GIS multiresource forest inventory*: Springer.

Korpela, I. (2004). Individual tree measurements by means of digital aerial Photogrammetry. *Silva Fennica*, 1-93.

Kumar, V. (2012). *Forest inventory parameters and carbon mapping from airborne LIDAR.* University of Twente Faculty of Geo-Information and Earth Observation (ITC), Enschede. Retrieved from http://www.itc.nl/library/papers_2012/msc/nrm/vinodkumar.pdf

Küng, O., Strecha, C., Beyeler, A., Zufferey, J., Floreano, D., Fua, P., & Gervaix, F. (2011). *The accuracy of automatic photogrammetric techniques on ultra-light UAV imagery.* Paper presented at the Proceedings of the International Conference on Unmanned Aerial Vehicle in Geomatics (UAV-g), Zurich, Switzerland.

Kuuluvainen, T. (1991). Relationships between crown projected area and components of above-ground biomass in Norway spruce trees in even-aged stands: empirical results and their interpretation. *Forest Ecology and Management, 40*(3), 243-260.

Kwak, D. A., Lee, W.-K., Cho, H.-K., Lee, S.-H., Son, Y., Kafatos, M., & Kim, S.-R. (2010). Estimating stem volume and biomass of Pinus koraiensis using LiDAR data. *Journal of plant research, 123*(4), 421-432.

Kwak, D. A., Lee, W. K., Lee, J. H., Biging, G. S., & Gong, P. (2007). Detection of individual trees and estimation of tree height using LiDAR data. *Journal of Forest Research, 12*(6), 425-434. doi: 10.1007/s10310-007-0041-9

Leberl, F., Irschara, A., Pock, T., Meixner, P., Gruber, M., Scholz, S., & Wiechert, A. (2010). Point Clouds: Lidar versus 3D Vision. *Photogrammetric Engineering and Remote Sensing, 76*(10), 1123-1134.

Leckie, D., Gougeon, F., Hill, D., Quinn, R., Armstrong, L., & Shreenan, R. (2003). Combined high-density lidar and multispectral imagery for individual tree crown analysis. *Canadian Journal of Remote Sensing, 29*(5), 633-649.

Lefsky, M., Cohen, W., Harding, D., Parker, G., Acker, S., & Gower, S. (2001). Lidar remote sensing of aboveground biomass in three biomes. *INTERNATIONAL ARCHIVES OF PHOTOGRAMMETRY REMOTE SENSING AND SPATIAL INFORMATION SCIENCES, 34*(3/W4), 155-162.

Lefsky, M. A., Cohen, W. B., Parker, G. G., & Harding, D. J. (2002). Lidar remote sensing for ecosystem studies. *Bioscience, 52*(1), 19-30. doi: 10.1641/0006-3568(2002)052[0019:lrsfes]2.0.co;2

Lemaire, C. (2008). *Aspects of the DSM production with high resolution images.* Paper presented at the Remote sensing and spatial information sciences, Beijing, China.

Lim, K. S., & Treitz, P. M. (2004). Estimation of above ground forest biomass from airborne discrete return laser scanner data using canopy-based quantile estimators. *Scandinavian Journal of Forest Research, 19*(6), 558-570. doi: 10.1080/02827580410019490

Lisein, J., Pierrot-Deseilligny, M., Bonnet, S., & Lejeune, P. (2013). A Photogrammetric Workflow for the Creation of a Forest Canopy Height Model from Small Unmanned Aerial System Imagery. *Forests, 4*(4), 922-944.

Lourakis, M. I., & Argyros, A. A. (2009). SBA: A software package for generic sparse bundle adjustment. *ACM Transactions on Mathematical Software (TOMS), 36*(1), 2.

Lovell, J., Jupp, D. L., Culvenor, D., & Coops, N. (2003). Using airborne and ground-based ranging lidar to measure canopy structure in Australian forests. *Canadian Journal of Remote Sensing, 29*(5), 607-622.

Lowe, D. G. (2004). Distinctive image features from scale-invariant keypoints. *International Journal of Computer Vision, 60*(2), 91-110.

Lu, D. S. (2006). The potential and challenge of remote sensing-based biomass estimation. *International Journal of Remote Sensing, 27*(7), 1297-1328. doi: 10.1080/01431160500486732

Lu, D. S., Mausel, P., Brondizio, E., & Moran, E. (2003). Classification of successional forest stages in the Brazilian Amazon basin. *Forest Ecology and Management, 181*(3), 301-312. doi: 10.1016/s0378-1127(03)00003-3

Madani, M. (2001). *Importance of Digital Photogrammetry for a complete GIS.* Paper presented at the 5th Global Spatial Data Infrastrucutre Conference, Catagena, Columbia.

Maharjan, S. (2012). *Estimation and mapping above ground woody carbon stocks using LIDAR data and digital camera imagery in the hilly forests of Gorkha, Nepal.* University of Twente Faculty of Geo-Information and Earth Observation (ITC), Enschede. Retrieved from http://www.itc.nl/library/papers_2012/msc/nrm/maharjan.pdf

Maltamo, M., Mustonen, K., Hyyppä, J., Pitkänen, J., & Yu, X. (2004). The accuracy of estimating individual tree variables with airborne laser scanning in a boreal nature reserve. *Canadian Journal of Forest Research, 34*(9), 1791-1801.

Map-gps-info.com. (2014). GPS accuracy – How Accurate is it? Retrieved 2014-02-01, 2014, from http://www.maps-gps-info.com/gps-accuracy.html

Maquaire, O., Malet, J. P., Remaitre, A., Locat, J., Klotz, S., & Guillon, J. (2003). Instability conditions of marly hillslopes: towards landsliding or gullying? The case of the Barcelonnette Basin, South East France. *Engineering Geology, 70*(1-2), 109-130. doi: 10.1016/s0013-7952(03)00086-3

McCullagh, M. (1988). Terrain and surface modelling systems: theory and practice. *The Photogrammetric Record, 12*(72), 747-779.

McGaughey, R. J., & Carson, W. W. (2003). Fusing LIDAR data, photographs, and other data using 2D and 3D visualization techniques. *Proceedings of Terrain Data: Applications and Visualization–Making the Connection*, 28-30.

Means, J. E. (2000). *Comparison of large-footprint and small-footprint lidar systems: design, capabilities, and uses.* Paper presented at the Proceedings of the Second International Conference on Geospatial Information in Agriculture and Forestry. Lake Buena Vista, Florida.

Means, J. E., Acker, S. A., Harding, D. J., Blair, J. B., Lefsky, M. A., Cohen, W. B., Harmon, M. E., & McKee, W. A. (1999). Use of large-footprint scanning airborne lidar to estimate forest stand characteristics in the Western Cascades of Oregon. *Remote Sensing of Environment, 67*(3), 298-308.

Merino, L., Caballero, F., Martínez-de-Dios, J. R., Maza, I., & Ollero, A. (2012). An unmanned aircraft system for automatic forest fire monitoring and measurement. *Journal of Intelligent & Robotic Systems, 65*(1-4), 533-548.

MOFSC (2009). Ministry of Forests and Soil Conservation, Government of Nepal.

Möller, M., Lymburner, L., & Volk, M. (2007). The comparison index: A tool for assessing the accuracy of image segmentation. *International Journal of Applied Earth Observation and Geoinformation, 9*(3), 311-321.

Morgan, J. L., Gergel, S. E., & Coops, N. C. (2010). Aerial Photography: A Rapidly Evolving Tool for Ecological Management. *Bioscience, 60*(1), 47-59. doi: 10.1525/bio.2010.60.1.9

Murtha, P., & Sharma, R. (2005). Remote sensing, photo interpretation and photogrammetry. *Forestry Handbook for British Columbia, fifth Ed., Vancouver, BC*, 657-662.

Næsset, E. (1997). Estimating timber volume of forest stands using airborne laser scanner data. *Remote Sensing of Environment, 61*(2), 246-253. doi: http://dx.doi.org/10.1016/S0034-4257(97)00041-2

Næsset, E., & Gobakken, T. (2005). Estimating forest growth using canopy metrics derived from airborne laser scanner data. *Remote Sensing of Environment, 96*(3–4), 453-465. doi: http://dx.doi.org/10.1016/j.rse.2005.04.001

Nakashizuka, T., Katsuki, T., & Tanaka, H. (1995). Forest Canopy Structure Analyzed by using Aerial Photographs. *Ecological Research, 10*(1), 13-18. doi: 10.1007/bf02347651

Natural Resources Canada. (2007). Natural Resources Canada. Government of Canada. Retrieved on 17 September 2013, http://www.nrcan.gc.ca/earthsciences/geomatics/satellite-imagery-air-photos/air-photos/about-aerialphotography/9687

Naumann, M., Geist, M., Bill, R., Niemeyer, F., & Grenzdörffer, G. (2013). Accuracy Comparison of Digital Surface Models Created by Unmanned Aerial Systems Imagery and Terrestrial Laser Scanner. *ISPRS-International Archives of the Photogrammetry, Remote Sensing and Spatial Information Sciences, 1*(2), 281-286.

Nguyet, D. A. (2012). *Error propagation in carbon estimation using the combination of airborne LIDAR data and very high resolution geo-eye satellite imagery in Ludhikhola watershed, Gorkha, Nepal.* University of Twente Faculty of Geo-Information and Earth Observation (ITC), Enschede. Retrieved from http://www.itc.nl/library/papers_2012/msc/nrm/danganhnguyet.pdf

Nilsson, M. (1996). Estimation of tree heights and stand volume using an airborne lidar system. *Remote Sensing of Environment, 56*(1), 1-7.

Nurminen, K., Karjalainen, M., Yu, X., Hyyppä, J., & Honkavaara, E. (2013). Performance of dense digital surface models based on image matching in the estimation of plot-level forest variables. *ISPRS Journal of Photogrammetry and Remote Sensing, 83*(0), 104-115. doi: http://dx.doi.org/10.1016/j.isprsjprs.2013.06.005

O'brien, R. M. (2007). A caution regarding rules of thumb for variance inflation factors. *Quality & Quantity, 41*(5), 673-690.

Okuda, T., Suzuki, M., Numata, S., Yoshida, K., Nishimura, S., Adachi, N., Niiyama, K., Manokaran, N., & Hashim, M. (2004). Estimation of aboveground biomass in logged and primary lowland rainforests using 3-D photogrammetric analysis. *Forest Ecology and Management, 203*(1–3), 63-75. doi: http://dx.doi.org/10.1016/j.foreco.2004.07.056

Packalen, P. (2009). *Using Airborne laser scanning data and digital aerial photographs to estimate growing stock by tree species.* (Doctoral thesis), University of Joensuu, Finland. Retrieved from http://www.metla.fi/dissertationes/df77.pdf

Patenaude, G., Milne, R., & Dawson, T. P. (2005). Synthesis of remote sensing approaches for forest carbon estimation: reporting to the Kyoto Protocol. *Environmental Science & Policy, 8*(2), 161-178. doi: 10.1016/j.envsci.2004.12.010

Persson, A., Holmgren, J., & Soderman, U. (2002). Detecting and measuring individual trees using an airborne laser scanner. *Photogrammetric Engineering and Remote Sensing, 68*(9), 925-932.

Picard, N., Saint-André, L., & Henry, M. (2012). Manual for building tree volume and biomass allometric equations: from field measurement to prediction.

Pignard, G., Dupouey, J.-L., Arrouays, D., & Loustau, D. (2000). Carbon stocks estimates for French forests. *BIOTECHNOLOGIE AGRONOMIE SOCIETE ET ENVIRONNEMENT, 4*(4), 285-289.

Pix4d. (2014). Pix4d simply powerful. Retrieved 2014-02-04, 2014, from http://www.pix4d.com

Popescu, S. C. (2007). Estimating biomass of individual pine trees using airborne lidar. *Biomass and Bioenergy, 31*(9), 646-655.

Popescu, S. C., & Wynne, R. H. (2004). Seeing the trees in the forest: Using lidar and multispectral data fusion with local filtering and variable window size for estimating tree height. *Photogrammetric Engineering and Remote Sensing, 70*(5), 589-604.

Popescu, S. C., Wynne, R. H., & Nelson, R. F. (2003). Measuring individual tree crown diameter with lidar and assessing its influence on estimating forest volume and biomass. *Canadian Journal of Remote Sensing, 29*(5), 564-577.

Pouliot, D., King, D., Bell, F., & Pitt, D. (2002). Automated tree crown detection and delineation in high-resolution digital camera imagery of coniferous forest regeneration. *Remote Sensing of Environment, 82*(2), 322-334.

Rabben, E., CHALMERS JÚNIOR, E., Manley, E., & PICKNP, P. (1960). Fundamentals of photo interpretation. *Manual of photographic interpretation*, 99-168.

Rapidlasso. (2013). Rapidlasso GnbH – fast tools to catch reality. Retrieved 2013-10-17, 2013, from http://www.rapidlasso.com

Razak, K. A., Straatsma, M. W., van Westen, C. J., Malet, J. P., & de Jong, S. M. (2011). Airborne laser scanning of forested landslides characterization: Terrain model quality and visualization. *Geomorphology, 126*(1-2), 186-200. doi: 10.1016/j.geomorph.2010.11.003

Reitberger, J., Heurich, M., Krzystek, P., & Stilla, U. (2007). Single tree detection in forest areas with high-density LiDAR data. *International Archives of Photogrammetry, Remote Sensing and Spatial Information Sciences, 36*(3), 139-144.

Reutebuch, S. E., McGaughey, R. J., Andersen, H.-E., & Carson, W. W. (2003). Accuracy of a high-resolution lidar terrain model under a conifer forest canopy. *Canadian Journal of Remote Sensing, 29*(5), 527-535.

Rutishauser, E., Noor'an, F., Laumonier, Y., Halperin, J., Hergoualch, K., & Verchot, L. (2013). Generic allometric models including height best estimate forest biomass and carbon stocks in Indonesia. *Forest Ecology and Management, 307*, 219-225.

Saez, J. L., Corona, C., Stoffel, M., Astrade, L., Berger, F., & Malet, J. P. (2012). Dendrogeomorphic reconstruction of past landslide reactivation with seasonal precision: the Bois Noir landslide, southeast French Alps. *Landslides, 9*(2), 189-203. doi: 10.1007/s10346-011-0284-6

Schardt, M., Hruby, W., Hirschmugl, M., Wack, R., & Franke, M. (2004). COMPARISON OF AERIAL PHOTOGRAPHS AND LASER SCANNING DATA AS METHODS FOR OBTAINING 3D FOREST STAND PARAMETERS. *International Archives of Photogrammetry, Remote Sensing and Spatial Information Sciences. Proceedings of the ISPRS working group VIII/2: Laser-Scanners for Forest and Landscape Assessment, 36*, 272-276.

Shiver, B. D., & Borders, B. E. (1996). *Sampling techniques for forest resource inventory*: John Wiley and Sons.

Shrestha, S. K. (2011). *Carbon stock estimation using very high resolution satellite imagery and individual crown segmentation : a case study of broadleaved and needle leaved forest of Dollakha, Nepal.* University of Twente Faculty of Geo-Information and Earth Observation (ITC), Enschede. Retrieved from http://www.itc.nl/library/papers_2011/msc/nrm/shrestha.pdf

Sierra, C. A., del Valle, J. I., Orrego, S. A., Moreno, F. H., Harmon, M. E., Zapata, M., Colorado, G. J., Herrera, M. A., Lara, W., Restrepo, D. E., Berrouet, L. M., Loaiza, L. M., & Benjumea, J. F. (2007). Total carbon stocks in a tropical forest landscape of the Porce region, Colombia. *Forest Ecology and Management, 243*(2-3), 299-309. doi: 10.1016/j.foreco.2007.03.026

Snavely, N., Seitz, S., & Szeliski, R. (2008). Modeling the World from Internet Photo Collections. *International Journal of Computer Vision, 80*(2), 189-210. doi: 10.1007/s11263-007-0107-3

Song, C. H., Dickinson, M. B., Su, L. H., Zhang, S., & Yaussey, D. (2010). Estimating average tree crown size using spatial information from Ikonos and QuickBird images: Across-sensor and across-site comparisons. *Remote Sensing of Environment, 114*(5), 1099-1107. doi: 10.1016/j.rse.2009.12.022

St-Onge, B., Vega, C., Fournier, R. A., & Hu, Y. (2008). Mapping canopy height using a combination of digital stereo-photogrammetry and lidar. *Int. J. Remote Sens., 29*(11), 3343-3364. doi: 10.1080/01431160701469040

St-Onge, B. A., & Achaichia, N. (2001). Measuring forest canopy height using a combination of lidar and aerial photography data. *INTERNATIONAL ARCHIVES OF PHOTOGRAMMETRY REMOTE SENSING AND SPATIAL INFORMATION SCIENCES, 34*(3/W4), 131-138.

Steininger, M. K. (2000). Satellite estimation of tropical secondary forest above-ground biomass: data from Brazil and Bolivia. *International Journal of Remote Sensing, 21*(6-7), 1139-1157. doi: 10.1080/014311600210119

Suárez, J.C. (2002). The use of remote sensing for operational forestry: the truth is out there. On ForestSAT symposium, Heriot Watt University, Edinburgh, 5th-9th August 2002. www.forestry.gov.uk/forestsat.

Swart, L. T. (2010). How the Up-to-date Height Model of the Netherlands (AHN) became a massive point data cloud. *NCG KNAW*, 17.

Tao, W., Lei, Y., & Mooney, P. (2011). *Dense point cloud extraction from UAV captured images in forest area.* Paper presented at the Spatial Data Mining and Geographical Knowledge Services (ICSDM), 2011 IEEE International Conference on.

Thapa, S. (2013). *Detection and mapping of incidence of Viscum Album in Pinus Sylvestris forest of southern French Alpe using satellite and airborne optical imagery.* University of Twente Faculty of Geo-Information and Earth Observation (ITC), Enschede. Retrieved from http://www.itc.nl/library/papers_2013/msc/nrm/thapa.pdf

Thenkabail, P. S., Enclona, E. A., Ashton, M. S., Legg, C., & De Dieu, M. J. (2004). Hyperion, IKONOS, ALI, and ETM plus sensors in the study of African rainforests. *Remote Sensing of Environment, 90*(1), 23-43. doi: 10.1016/j.rse.2003.11.018

Thiery, Y., Malet, J. P., Sterlacchini, S., Puissant, A., & Maquaire, O. (2007). Landslide susceptibility assessment by bivariate methods at large scales: Application to a complex mountainous environment. *Geomorphology, 92*(1-2), 38-59. doi: 10.1016/j.geomorph.2007.02.020

Thomas, V., Treitz, P., McCaughey, J., & Morrison, I. (2006). Mapping stand-level forest biophysical variables for a mixedwood boreal forest using lidar: an examination of scanning density. *Canadian Journal of Forest Research, 36*(1), 34-47.

Tiwari, A. K., & Singh, J. S. (1984). Mapping forest biomass in India through aerial photographs and nondestructive field sampling. *Applied Geography, 4*(2), 151-165. doi: http://dx.doi.org/10.1016/0143-6228(84)90019-5

Triggs, B., McLauchlan, P. F., Hartley, R. I., & Fitzgibbon, A. W. (2000). Bundle adjustment—a modern synthesis *Vision algorithms: theory and practice* (pp. 298-372): Springer.

Valbuena, R., Fernández de Sevilla, T., Mauro, F., Pascual, C., García-Abril, A., Martín-Fernández, S., & Manzanera, J. A. (2008). Lidar and true-orthorectification of infrared aerial imagery of high Pinus sylvestris forest in mountainous relief. In *Proc. 8th Int. Conf. LiDAR Appl. Forest Assess. Inventory SilviLaser* (pp. 17-19)

Verhoeven, G. (2011). Taking computer vision aloft–archaeological three-dimensional reconstructions from aerial photographs with photoscan. *Archaeological Prospection, 18*(1), 67-73.

Wang, L., Gong, P., & Biging, G. S. (2004). Individual tree-crown delineation and treetop detection in high-spatial-resolution aerial imagery. *Photogrammetric Engineering and Remote Sensing, 70*(3), 351-358.

Waring, R. H., & Schlesinger, W. H. (1985). *Forest ecosystems : concepts and management / Richard H. Waring, William H. Schlesinger*: Orlando : Academic Press, 1985.

Waser, L., Baltsavias, E., Ecker, K., Eisenbeiss, H., Feldmeyer-Christe, E., Ginzler, C., Küchler, M., & Zhang, L. (2008). Assessing changes of forest area and shrub encroachment in a mire ecosystem using digital surface models and CIR aerial images. *Remote Sensing of Environment, 112*(5), 1956-1968.

Watt, M. S., & Kirschbaum, M. U. (2011). Moving beyond simple linear allometric relationships between tree height and diameter. *Ecological Modelling, 222*(23), 3910-3916.

Weber, D. (1994). Research into earth movements in the Barcelonnette basin. *Temporal Occurence and Forecasting of Landslides in the European Community*, 321-336.

Weir, M. J. (2000). Acquisition of Spatial Data by Forest Management Agencies. *Quantifying Spatial Uncertainty in Natural Resources: Theory and Applications for GIS and Remote Sensing*, 103.

Wolf, P. R., & Dewitt, B. A. (2000). *Elements of photogrammetry : with applications in GIS*. Boston etc.: McGraw-Hill.

Workie, T. G. (2011). *Assessment of aboveground carbon stock in coniferous and broadleaf forests, using high spatial resolution satellite images.* University of Twente Faculty of Geo-Information and Earth Observation (ITC), Enschede. Retrieved from http://www.itc.nl/library/papers_2011/msc/gem/workie.pdf

Yu, Q., Gong, P., Clinton, N., Biging, G., Kelly, M., & Schirokauer, D. (2006). Object-based detailed vegetation classification with airborne high spatial resolution remote sensing imagery. *Photogrammetric Engineering and Remote Sensing, 72*(7), 799.

Yu, X., Hyyppä, J., Hyyppä, H., & Maltamo, M. (2004). Effects of flight altitude on tree height estimation using airborne laser scanning. *Proceedings of the Laser Scanners for Forest and Landscape Assessment–Instruments, Processing Methods and Applications*, 02-06.

Yu, Y., Saatchi, S., Heath, L. S., LaPoint, E., Myneni, R., & Knyazikhin, Y. (2010). Regional distribution of forest height and biomass from multisensor data fusion. *Journal of Geophysical Research: Biogeosciences (2005–2012), 115*(G2).

Zhan, Q., Molenaar, M., Tempfli, K., & Shi, W. (2005). Quality assessment for geo-spatial objects derived from remotely sensed data. *International Journal of Remote Sensing, 26*(14), 2953-2974.

Zhang, X., Feng, X., & Jiang, H. (2010). Object-oriented method for urban vegetation mapping using IKONOS imagery. *International Journal of Remote Sensing, 31*(1), 177-196.

Zhao, K., Popescu, S., & Nelson, R. (2009). Lidar remote sensing of forest biomass: A scale-invariant estimation approach using airborne lasers. *Remote Sensing of Environment, 113*(1), 182-196.

Appendices

Appendix 1: Distribution of sampling plots

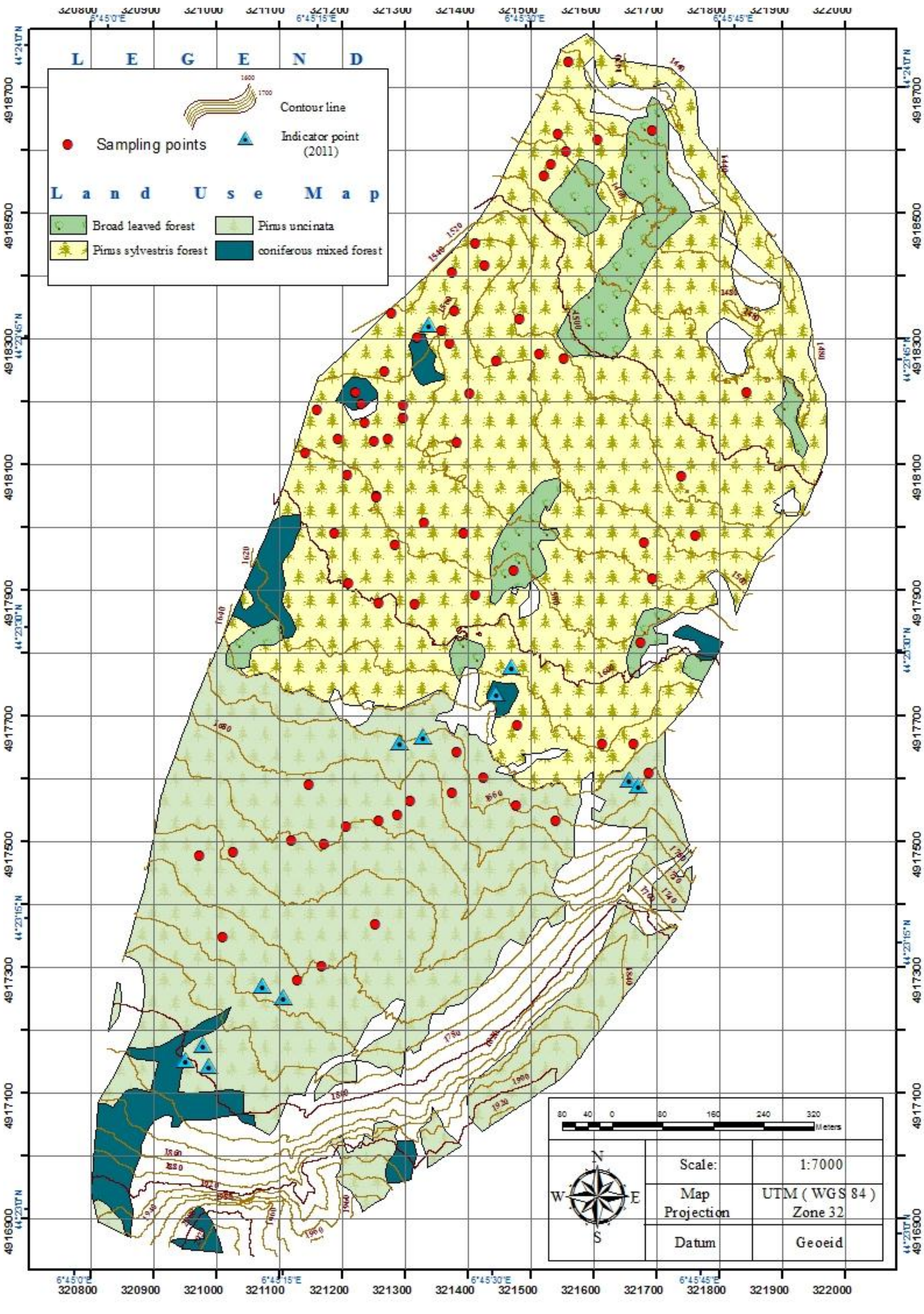

Appendix 2: Slope correction table

Plot size 500 m2

Slope%	Radius(m)	Slope%	Radius(m)	Slope%	Radius(m)
0	12.62				
1	12.62	36	13.01	71	13.97
2	12.62	37	13.03	72	14
3	12.62	38	13.05	73	14.04
4	12.62	39	13.07	74	14.07
5	12.62	40	13.09	75	14.1
6	12.63	41	13.12	76	14.14
7	12.63	42	13.14	77	14.17
8	12.64	43	13.16	78	14.21
9	12.64	44	13.19	79	14.24
10	12.65	45	13.21	80	14.28
11	12.65	46	13.24	81	14.31
12	12.66	47	13.26	82	14.35
13	12.67	48	13.29	83	14.38
14	12.68	49	13.31	84	14.42
15	12.69	50	13.34	85	14.45
16	12.7	51	13.37	86	14.49
17	12.71	52	13.39	87	14.52
18	12.72	53	13.42	88	14.56
19	12.73	54	13.45	89	14.6
20	12.74	55	13.48	90	14.63
21	12.75	56	13.51	91	14.67
22	12.77	57	13.53	92	14.71
23	12.78	58	13.56	93	14.74
24	12.79	59	13.59	94	14.78
25	12.81	60	13.62	95	14.82
26	12.82	61	13.65	96	14.85
27	12.84	62	13.68	97	14.89
28	12.86	63	13.72	98	14.93
29	12.87	64	13.75	99	14.97
30	12.89	65	13.78	100	15
31	12.91	66	13.81	101	15.04
32	12.93	67	13.84	102	15.08
33	12.95	68	13.87	103	15.12
34	12.97	69	13.91	104	15.15
35	12.99	70	13.94	105	15.19

Source: Y.A. Hussin (2001) from lecture note

Appendix 3: Image-registration table

Link	X Source	Y Source	X Map	Y Map	Residual_x	Residual_y	Residual
1	321546.24	4918761.22	321545.99	4918760.62	0.340357	-0.108698	0.357293
2	321586.68	4918746.98	321585.73	4918746.79	-0.499966	0.14519	0.520621
3	321611.51	4918710.48	321611.16	4918710.08	-0.025512	0.0516513	0.057608
4	321601.97	4918711.87	321601.87	4918711.51	0.253241	0.139806	0.289269
5	321607.05	4918710.34	321606.48	4918709.77	-0.23701	-0.10042	0.257407
6	321652.96	4918712.37	321652.99	4918712.31	0.240507	0.0989228	0.260056

Appendix 4: Histograms of field measurements

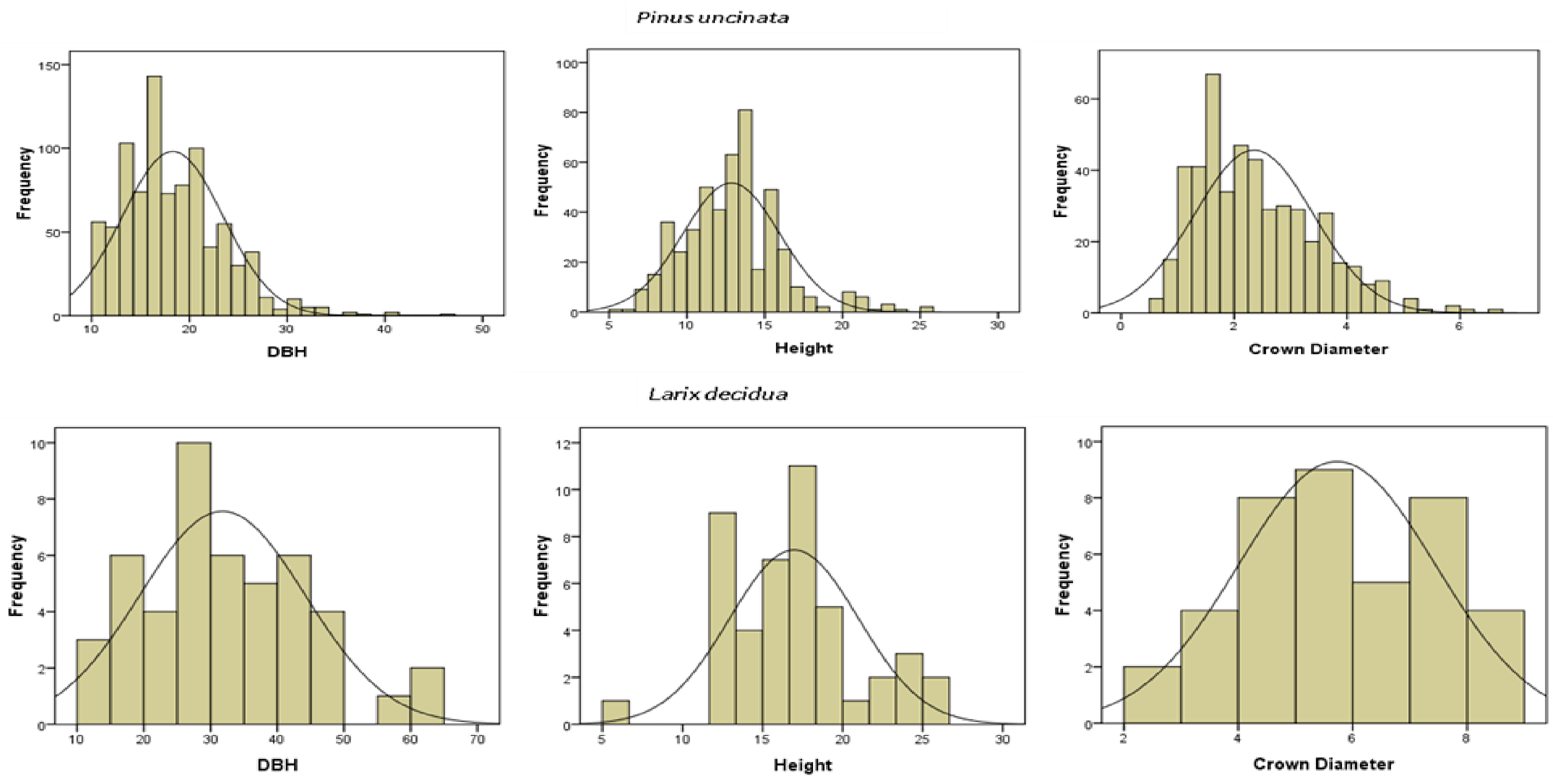

Appendix 4: Histogram of field measurements

Fagus sylvatica

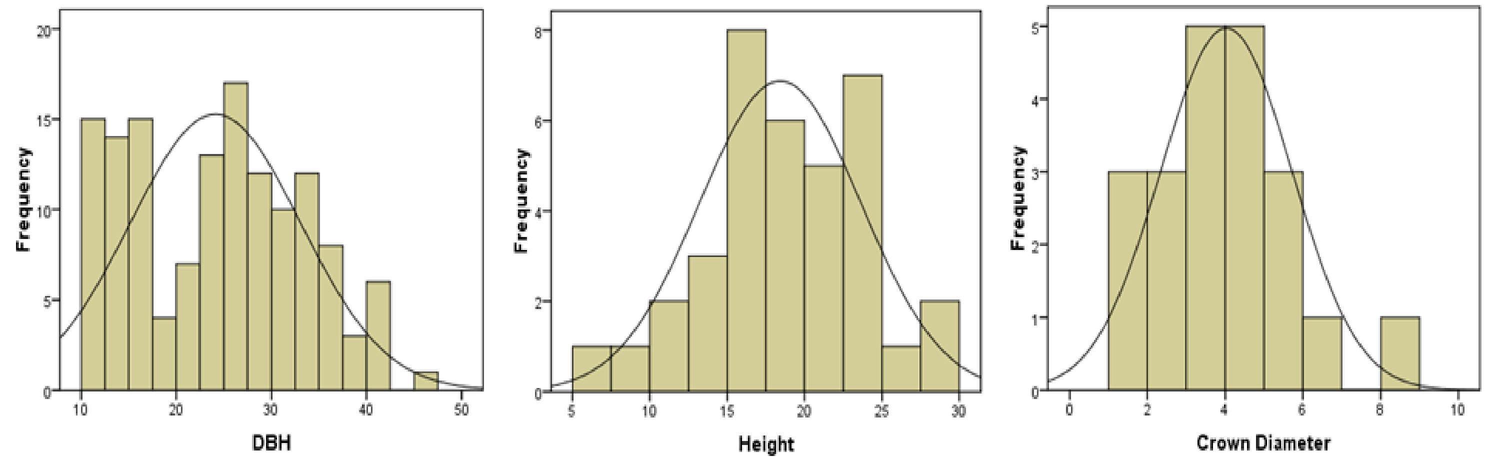

Appendix 5: Details of ANOVA table

SUMMARY

Groups	Count	Sum	Average	Variance
Aerial derived height	340	3813.37	11.2158	6.61692
LiDAR derived height	340	4006.307	11.7833	7.380725

ANOVA

Source of Variation	SS	df	MS	F	P-value	F crit
Between Groups	54.74225	1	54.7422	7.821637	0.005309	3.855211
Within Groups	4745.201	678	6.99882			
Total	4799.944	679				

Appendix 6: Details of ANOVA table and regression parameters

For aerial image

Pinus Uncinata

ANOVA

	df	*SS*	*MS*	*F*	*Significance F*
Regression	2	11.15332	5.576662	37.92506	3.43E-12
Residual	77	11.32241	0.147044		
Total	79	22.47573			

Regression coefficients

	Coefficients	*Standard Error*	*t Stat*	*P-value*	*Lower 95%*	*Upper 95%*
Intercept	-0.543	0.466	-1.164	0.247795	-1.473	0.385
CHM	1.287	0.195	6.602	4.67E-09	0.899	1.676
CPA	0.514	0.128	4.005	0.000141	0.258	0.77

Pinus sylvestris

ANOVA

	df	*SS*	*MS*	*F*	*Significance F*
Regression	2	15.59128	7.79564	28.563	1.07E-09
Residual	67	18.28595	0.27293		
Total	69	33.87723			

Regression coefficients

	Coefficients	*Standard Error*	*t Stat*	*P-value*	*Lower 95%*	*Upper 95%*
Intercept	0.397	0.553	0.718	0.47495	-0.707	1.503
CHM	1.062	0.217	4.884	6.77E-06	0.628	1.496
CPA	0.721	0.146	4.919	5.93E-06	0.429	1.0149

Fagus sylvatica

ANOVA

	df	*SS*	*MS*	*F*	*Significance F*
Regression	2	8.471265	4.23563	60.465	2.61E-07
Residual	13	0.910663	0.07005		
Total	15	9.381928			

Regression coefficients

	Coefficients	*Standard Error*	*t Stat*	*P-value*	*Lower 95%*	*Upper 95%*
Intercept	-3.184	0.672	-4.734	0.00039	-4.637	-1.731
CHM	2.287	0.295	7.749	3.16E-06	1.649	2.925
CPA	0.701	0.175	4.001	0.00151	0.322	1.078

Larix decidua

ANOVA

	df	*SS*	*MS*	*F*	*Significance F*
Regression	2	13.21249	6.60625	25.9986	0.000575
Residual	7	1.778702	0.2541		
Total	9	14.99119			

Regression coefficients

	Coefficients	*Standard Error*	*t Stat*	*P-value*	*Lower 95%*	*Upper 95%*
Intercept	-1.959	1.144	-1.711	0.13	-4.666	0.747
CPA	0.332	0.19	1.741	0.125	-0.118	0.783
CHM	2.316	0.52	4.449	0.002	1.085	3.547

For LiDAR

Pinus uncinata

ANOVA

	df	*SS*	*MS*	*F*	*Significance F*
Regression	2	9.920921	4.96046	33.4032	3.59E-11
Residual	77	11.4347	0.1485		
Total	79	21.35562			

Regression coefficients

	Coefficients	*Standard Error*	*t Stat*	*P-value*	*Lower 95%*	*Upper 95%*
Intercept	-0.804	0.532	-1.509	0.135	-1.865	0.256
CHM	1.545	0.225	6.836	1.69E-09	1.095	1.995
CPA	0.361	0.106	3.387	0.00112	0.148	0.573

Pinus sylvestris

ANOVA

	df	*SS*	*MS*	*F*	*Significance F*
Regression	2	19.77076	9.88538	25.8389	4.81E-09
Residual	67	25.63266	0.38258		
Total	69	45.40342			

Regression coefficients

	Coefficients	*Standard Error*	*t Stat*	*P-value*	*Lower 95%*	*Upper 95%*
Intercept	-0.152	0.68	-0.223	0.823	-1.511	1.206
CPA	0.157	0.09	1.735	0.087	-0.023	0.338
CHM	1.789	0.288	6.208	3.84E-08	1.214	2.365

Fagus sylvatica

ANOVA

	df	*SS*	*MS*	*F*	*Significance F*
Regression	2	9.996631	4.99832	57.5584	3.48E-07
Residual	13	1.128907	0.08684		
Total	15	11.12554			

Regression coefficients

	Coefficients	*Standard Error*	*t Stat*	*P-value*	*Lower 95%*	*Upper 95%*
Intercept	-3.479	0.706	-4.926	0.0002	-5.005	-1.953
CHM	2.036	0.248	8.202	1.70E-06	1.5	2.572
CPA	0.925	0.246	3.76	0.002	0.393	1.456

Larix decidua

ANOVA

	df	*SS*	*MS*	*F*	*Significance F*
Regression	2	9.135316	4.56766	9.41899	0.01035
Residual	7	3.394589	0.48494		
Total	9	12.5299			

Regression coefficients

	Coefficients	*Standard Error*	*t Stat*	*P-value*	*Lower 95%*	*Upper 95%*
Intercept	-1.634	2.214	-0.738	0.484	-6.87	3.6
CPA	0.395	0.388	1.017	0.342	-0.523	1.313
CHM	2.146	1.073	1.999	0.085	-0.392	4.686

Appendix 7: Carbon stock map of the study area using aerial images

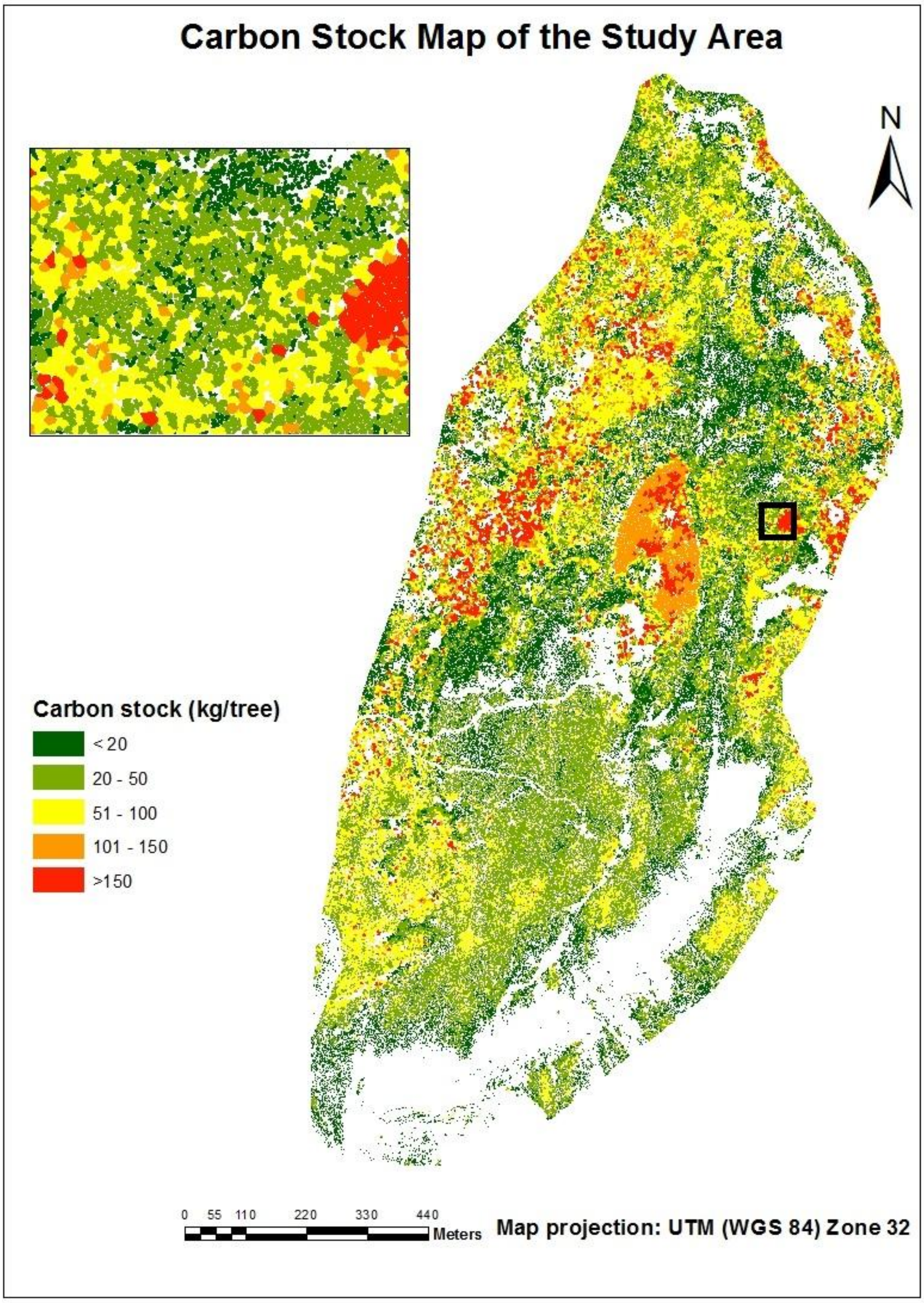

Appendix 8: Field measurements (small experiment around ITC)

	Height measurement in meter		
Observations	Theodolite	LiDAR	Haga hypsometer
1	11.4	11.12	11.25
2	10.83	10.39	11
3	24.83	25.47	24.5
4	12.58	12.06	13
5	10.19	10.24	10.5
6	24.38	24.14	27.75
7	23.91	21	23.5
8	19.16	17.78	20.25
9	7.88	7.56	8
10	18.42	19.5	19.5

Appendix 9: Summary of statistics

Statistic	Height obtained from		
	Theodolite (m)	LiDAR (m)	Haga (m)
Mean	16.36	15.93	16.93
Minimum	7.88	7.56	8.00
Maximum	24.83	25.47	27.75
Std Deviation	6.54	6.42	6.99
Observations	10	10	10

Appendix 10: Field photographs